STOKES SPECTROSCOPY: THE DEVELOPMENT OF A NOVEL METHOD TO ACQUIRE AND INTERPRET POLARIZED EMISSION SPECTRA – APPLICATIONS TO POLY(3HEXYLTHIOPHENE) AND P(NDI2OD-T2)

by

STEVEN V. ULRICH

PAULO T. ARAUJO, COMMITTEE CHAIR
NEWTON BARBOSA
ADAM HAUSER
MATTHIAS KAMINSKI
GARY MANKEY

A DISSERTATION

Submitted in partial fulfillment of the requirements
for the degree of Doctor of Philosophy
in the Department of Physics and Astronomy
in the Graduate School of
The University of Alabama

TUSCALOOSA, ALABAMA

2018

ABSTRACT

Optics, as a field of study, has been a critical tool within the discipline of material science for over one hundred years. Through lights interaction with matter, researchers can determine information such as material composition, electronic and physical properties. This information is then used to guide research for specific applications. From the outside, it may seem as though optics as a field is complete; all possible experiments known and possible outcomes interpreted. However, one such property of light, specifically polarization, has proven difficult to measure and subsequently analyze in a meaningful way. Current techniques for measuring polarization information involve simple rotations of a linear polarizer, or analyzer, to get a loose understanding of an emitting sources polarization state. However, this technique and others like it are far from complete and much of the polarization information is still unavailable to researchers. One way to elucidate more polarization information is to implement a method proposed by Stokes in the late 1800s, in which four parameters are used to describe a sources intensity and polarization states. The goal of this work is to show how the addition of the Stokes technique to a typical spectroscopic setup, along with computational fitting, produces direct measurements of these polarization states. Further, we show the capabilities of these adaptations by applying the technique to two organic semi-conducting polymers, Poly(3-hexothilophene) and P(NDI2OD-T2). Doing so has allowed for further elucidation of material properties, including aggregate formation and energy transfer, which is typically unavailable for such materials at high temperature.

DEDICATION

To claim that this work was solely accomplished through my own blood, sweat, and tears would be a huge disservice to the many individuals that helped me in their own ways throughout this process. For this reason; I dedicate this work to my family who served as my foundation and gave me a place to retreat when things seemed impossible. To my friends who reminded me that it is important to remain goofy and take things a little less seriously. Finally, my career advisors and colleagues, who showed me that no barrier is too high when you put your nose to the grindstone and are filled with a passion for learning.

LIST OF ABBREVIATIONS AND SYMBOLS

EM	Electromagnetic
λ	Wavelength
ν	Frequency
c	Speed of light in a vacuum.
nm	Nanometer
P3HT	Poly(3hexylthiophene)
NDI	P(NDI2OD-T2)
p-type	Positive charge carrier
n-type	Negative charge carrier
E_n	Electric field of a light source in the "n" direction (n=x,y).
ω	Angular frequency
t	Time
κ	Wave number
z	Distance variable in the "z" direction.
δ_n	Phase angle in the "n" direction (n=x,y).
cos	Cosine trigonometric function
sin	Sine trigonometric function
I	Total intensity of emitted light in Watts.
S_0	Stokes parameter signifying the total intensity.

S_1	Stokes parameter determining the amount of horizontal or vertical polarized emission (positive or negative numbers respectively)
S_2	Stokes parameter determining the amount of positive or negative 45º polarized emission (positive or negative numbers respectively)
S_3	Stokes parameter determining the amount of right or left circular polarized emission (positive or negative numbers respectively)
$\vec{S}$	Stokes Vector
m_{ij}	Matrix element for the i-j cell of the matrix. "i" noting the column, "j" the row.
M_a	Matrix representing the optical element "a" within the Stokes formalism.
p	Attenuation parameter for an optical element within the Stokes formalism.
θ	Angular position / rotation
mm	milimeter
L.P.	Linear Polarizer optical element
Q.W.P.	Quarter Wave Plate optical element
H.W.P.	Half Wave Plate optical element
CCD	Charge Coupled Device
d	Transmission grating slit separation
m	Integer number representing the bright fringe order after passing through a transmission grating
β	Resulting angle between reflected m^{th} order transmission and straight line from grating normal.
T.G.	Transmission Grating
ϕ	Angle between Transmission Grating and Mirror planes.
FL	Fluorescence
PL	Photoluminescence

HOMO	Highest Occupied Molecular Orbital
LUMO	Lowest Unoccupied Molecular Orbital
A_n	Singlet state energy level A, with n denoting the n=0,1,2… state. 0 being the ground state, 1 and above excited states.
n	n^{th} vibrational mode.
UV	Ultra Violet radiation
NIR	Near-infrared radiation
$\vec{M}$	Transition moment of a molecule
IR	Infrared radiation
RAIRS	Reflection-absorption infrared spectroscopy
mg	Milligram
mL	Milliliter
AFM	Atomic Force Microscopy
TEM	Transmission Electron Microscopy
H	Hamiltonian operator
V	Potential energy operator
ψ	Wavefunction
A	Antisymmetrization operator
c_j	Coefficients obtained through variational principle
ΔD	Difference between the energy shift of the ground and excited state
J_0	Energy associated with the interaction between neighboring molecules (resonance energy)
k	Periodic boundary condition
IC	In P(NDI2OD-T2): intrachain species

Agg	Aggregate
Agg I	In P(NDI2OD-T2): first aggregate species
Agg II	In P(NDI2OD-T2): second aggregate species
CN	Chloronaphthalene
DCB	DiChlorobenzene
PD	Polarization Degree
UP	Unpolarized contribution (equal to 1-PD)
IA	Integrated Area
β	Related to the correlation length by $l_0 = \frac{1}{\ln(\beta)}$
l_0	Correlation length of a polymer
σ	Linewidth of fit gaussian peak
eV	Electron-Volt
N_{coh}	Exciton coherence number
S	Huang-Rhys parameter

ACKNOWLEDGEMENTS

It is my absolute pleasure to take this moment to thank my dissertation chair, Paulo Araujo for all his help and work throughout this process. You've been the catalyst through which my hard work has come to fruition over these past five years, and have helped me understand hard questions throughout. I would also like to give my sincerest thanks to my committee members; Gary Mankey, Adam Hauser, Matthias Kaminski, and Newton Barbosa, for helping me throughout the project and in my professional career. I would also like to thank Matthias Schweizer, for helping me with initial laboratory setup and testing, Huan Nyugen and Sean McCracken for helping me with measurements and continuing on the project following my graduation.

I'd also like to take a moment to thank my family, through your example, all of this became possible.

CONTENTS

LIST OF TABLES

LIST OF FIGURES

1. INTRODUCTION

Optics, as a field of study, is the consideration of how propagating electromagnetic (EM) radiation, or light, interacts with matter. Traditionally; scientists describe light using wave mechanics, and through this description can break light into a spectrum based upon its wavelength (λ), or it's frequency (ν), which are related to each other and the speed of light (c) by $c = \lambda\nu$ in vacuum[1-4]. The electromagnetic spectrum, broken up into colloquial names based upon the wavelength and frequency, is shown below in Figure 1.

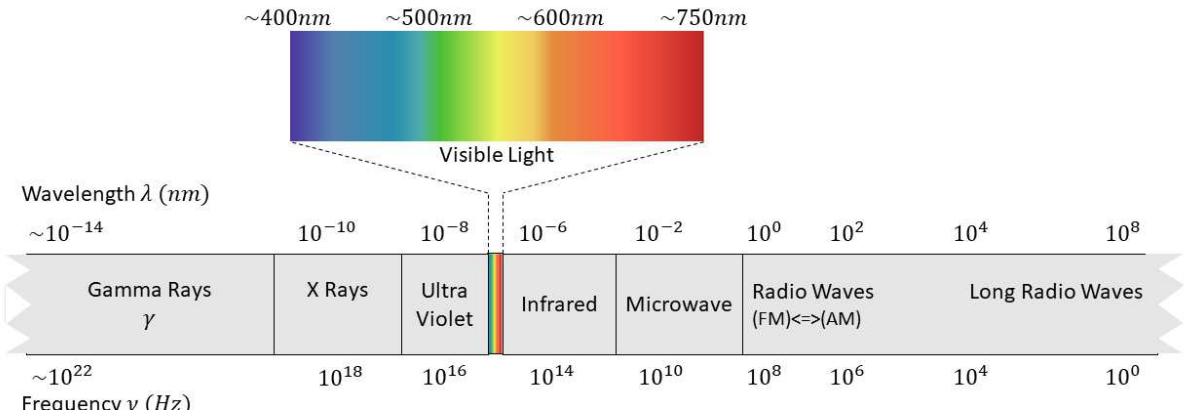

Figure 1. Electromagnetic Spectra

Optical measurements have been at the forefront of experimental techniques used by researchers for centuries [1-6]. Depending on the nature of the application, or what properties a researcher is seeking to elucidate, different regions of the electromagnetic field can be of use. For example, microwaves are utilized for heating as they are within the length scale that allows molecules (particularly water) to oscillate. X-Rays cause calcium to luminescence, which upon collection can be used to examine a patient's skeletal structure for medical tests [1-6]. These examples are only a tiny subset of possible applications that are possible, with different regions of the optical spectra being useful for various applications and experiments.

Within the field of condensed and soft matter physics, researchers tend to spend their time on optical phenomena such as Raman shifts, Photoluminescence, and Absorbance when probing materials. These phenomena have direct implications to a given materials formation and electronic states among other interesting properties [1-6]. Given the length scales associated with these phenomena, it is useful to consider optical disturbances within or around the visible spectra (~400-750nm), although this is not a hard and fast rule. Traditional optical measurements within this framework follow the same basic principles: illuminate (or excite) a sample with a known external EM source (often times a laser), collect resulting optical disturbances, and analyze to see what, if anything, has changed. Depending on the nature of the collected optical response, researchers can get an idea of the physical and electronic nature of the material in question or any phenomena that might be present through the induced excitation.

Soft matter materials are an exemplary candidate for such optical measurements. Specifically, photoluminescence and absorption measurements have proven useful for understanding the electronic and physical properties of organic semi-conducting polymers [6-11]. These measurements provide information, which can be subsequently used to apply these polymers in devices such as LEDs, Solar Cells, and transistors [7-9, 12-20]. Two such organic polymers, which have been in the forefront of research are poly(3hexylthiophene) (abbreviated P3HT) a p-type conjugated polymer and P(NDI2OD-T2) (abbreviated NDI) a n-type conjugated polymer ("p" and "n" determine the charge carrier). P3HT has a particularly rich background, with a plethora of information about formation and electronic properties [16, 21-33]. Conversely, NDI serves as a new player in the field, and is of great interest as a useful n-type polymer, which have proven difficult to come by (mainly due to functionalization considerations) [34-38].

This dissertation focuses its attention on adapting traditional optical measurements, particularly luminescence and Raman, to account for a traditionally difficult optical property to measure: polarization. This is done through application of a formalism for polarized emission given by Sir Gregory Stokes in the 1800s [1, 2, 5]. Applying this approach, we will show how previously discovered information can be acquired within this new framework, while eliminating normal restrictions such as the need for low

temperatures, and specific film processing. Additionally, we will show how additional information regarding polymer organization, namely aggregation, can be understood within stokes polarization framework. First, we will establish understanding of the Stokes formalism and the laboratory adaptations necessary to acquire polarization dependent spectra. Then, general background information on luminescence and polymers, with emphasis on the organic conjugated polymers P3HT and NDI, is provided. Finally, we provide research papers which document the application of Stokes Spectroscopy to P3HT, NDI. These papers have and or will be submitted to peer reviewed journals. Additionally, we provide future work for this technique, additional findings which require more work / consideration, and an overall outlook for the application.

2. EXPERIMENTAL SETUP AND METHODS

a. The Stokes Formalism for polarized light

The Stokes parameters of polarization arose through the efforts provided by Sir George Gabriel Stokes in 1852 [1, 2, 10]. The goal: to expand upon the seminal work by Augustin-Jean Fresnel describing the polarized nature of light [1, 2, 4, 10]. Specifically, Fresnel's work described light as transverse components following a propagation direction; these transverse components could be utilized to form a so-called *polarization ellipse* [1, 2, 4, 10]. While complete mathematically, direct measurements following this formalism were impossible due to equipment and method limitations [1, 2, 4, 10]. Stokes however found a way to describe light through four distinct parameters; one describing the total intensity of the light source, and three polarization components describing the vertical / horizontal polarization, the ±45º polarization, and the left / right circular polarization. This realization made it possible to simultaneously obtain information of an emitting light sources energy and polarized / un-polarized states [1, 2, 10].

To determine the Stokes parameters of polarization, we consider light propagating in the z-direction. With this propagation direction, we can describe transverse oscillations of the beams electric field (E) in the x and y direction respectively as:

$$E_x(z,t) = E_{ox}\cos[\omega t - \kappa z + \delta_x] \quad (1a)$$
$$E_y(z,t) = E_{oy}\cos[\omega t - \kappa z + \delta_y] \quad (1b)$$

The subscripts x and y specify dependence to the respective transverse direction. ω and κ are the angular frequency and wave number of the emitted light, and therefore, $\omega t - \kappa z$ is used to describe the position and time depend amplitude of the electric field. δ serves as an arbitrary phase which is set upon emission (however it can change with time if necessary). E_{on} $(n = x, y)$, is the maximum amplitude of

the electric field in that particular direction. It is possible to form an ellipse (aptly named the polarization ellipse) with these two transverse components. To do so, one needs to map on an x-y plane the particular value of the electric field in the x- and y- direction. Doing this for all space and time yields the desired ellipse, mathematically we can do this by re-writing the above equations as follows:

$$\frac{E_x(z,t)}{E_{ox}} = \cos[\omega t - \kappa z + \delta_x] \tag{2a}$$

$$\frac{E_y(z,t)}{E_{oy}} = \cos\left[\omega t - \kappa z + \delta_y\right]. \tag{2b}$$

Using the following identity; $\cos(A+B) = \cos(A)\cos(B) - \sin(A)\sin(B)$, we can re-write the above as follows:

$$\frac{E_x(z,t)}{E_{ox}} = \cos[\omega t - \kappa z]\cos[\delta_x] - \sin[\omega t - \kappa z]\sin[\delta_x] \tag{3a}$$

$$\frac{E_y(z,t)}{E_{oy}} = \cos[\omega t - \kappa z]\cos\left[\delta_y\right] - \sin[\omega t - \kappa z]\sin\left[\delta_y\right]. \tag{3b}$$

From here, multiply both 3a and 3b by $\sin[\delta_y]$ and $\sin[\delta_x]$ respectively. Doing so yields:

$$\frac{E_x(z,t)}{E_{ox}}\sin[\delta_y] = \cos[\omega t - \kappa z]\cos[\delta_x]\sin[\delta_y] - \sin[\omega t - \kappa z]\sin[\delta_x]\sin[\delta_y] \tag{4a}$$

$$\frac{E_y(z,t)}{E_{oy}}\sin[\delta_x] = \cos[\omega t - \kappa z]cos[\delta_y]\sin[\delta_x] - \sin[\omega t - \kappa z]sin[\delta_y]\sin[\delta_x]. \tag{4b}$$

Here, we notice that the last terms of both 4a and 4b are the same, we can combine 4a and 4b yielding (note that the following identity was used while combining: $\sin[A]\cos[B] - \sin[A]\cos[B] = \sin[A-B]$):

$$\frac{E_x(z,t)}{E_{ox}}\sin\left[\delta_y\right] - \frac{E_y(z,t)}{E_{oy}}\sin[\delta_x] = \cos[\omega t - \kappa z]\sin\left[\delta_y - \delta_x\right]. \tag{5}$$

Doing the same to equations 3a and 3b, instead using the opposing equations $cos[\delta_n]$ $(n = x, y)$, one arrives at (using the same identity as above):

$$\frac{E_x(z,t)}{E_{ox}}\cos\left[\delta_y\right] - \frac{E_y(z,t)}{E_{oy}}\cos[\delta_x] = \sin[\omega t - \kappa z]\sin\left[\delta_y - \delta_x\right]. \tag{6}$$

Squaring both equation 5 and 6, then adding brings us to:

$$\frac{E_x^2(z,t)}{E_{ox}^2} + \frac{E_y^2(z,t)}{E_{oy}^2} - 2\frac{E_x}{E_{ox}}\frac{E_y}{E_{oy}}\cos[\delta] = \sin^2[\delta], \tag{7}$$

where $\delta = \delta_y - \delta_x$.

Equation 7, should be recognizable as that of an ellipse, mapping the x- and y- position of the electric field vector to the x-y plane to a particular position as time and position are varied. This ellipse is referred to by Stokes as the *polarization ellipse* of propagating emission [1, 2, 10].

To form the Stokes parameters of polarization, we again consider the transverse components of an optical disturbance propagating in the z-direction:

$$E_x(t) = E_{ox}(t)\cos[\omega t + \delta_x(t)] \tag{8a}$$
$$E_y(t) = E_{oy}(t)\cos\left[\omega t + \delta_y(t)\right]. \tag{8b}$$

This light need not be monochromatic, which is of particular importance for this projects work (more on this later). Additionally, the use of a wave number (κ) is not necessary as we are considering measured light. Therefore, the translational position (z) is known, meaning this value can be folded into the respective time dependent phase factor $(\delta_n(t);\ n = x, y)$. We must also explicitly note that the phase factors and the electric field amplitudes may vary with time, however these values are assumed to vary slowly when compared to the oscillation of the optical disturbance (this information is within the cosine factor). Following the same steps outlined above, we can use equation 8a and 8b to form a polarization ellipse:

$$\frac{E_x^2(t)}{E_{ox}^2(t)} + \frac{E_y^2(t)}{E_{oy}^2(t)} - 2\frac{E_x(t)}{E_{ox}(t)}\frac{E_y(t)}{E_{oy}(t)}\cos[\delta(t)] = \sin^2[\delta(t)] \tag{9}$$

again, $\delta(t) = \delta_y(t) - \delta_x(t)$ is an arbitrary phase difference between the two transverse components.

For convenience, we consider monochromatic disturbances. Doing so allows us to realize that the initial amplitudes $(E_{on}^2(t); n = x, y)$ and phase constants remain constant for all time, allowing us to rewrite Equation 9 as:

$$\frac{E_x^2(t)}{E_{ox}^2}+\frac{E_y^2(t)}{E_{oy}^2}-2\frac{E_x(t)}{E_{ox}}\frac{E_y(t)}{E_{oy}}\cos[\delta]=\sin^2[\delta]\,. \tag{9}$$

Note that $E_n^2(t);\ (n=x,y)$ remains time dependent, this is due to the fact that we still are yet to take a measurement, or more specifically the time at which we take a measurement determines that amplitude at that given point in time. This would be a problem, if physical measurements were on the same order as a visible waves oscillation period ($\sim 10^{-15}s$). Because that isn't the case for our experiment, we take the time average of the measured electric field amplitudes:

$$\langle E_n(t)E_m(t)\rangle=\lim_{T\to\infty}\int_0^T E_n(t)E_m(t)dt\,;\quad n,m=x,y \tag{10}$$

with solutions of:

$$\lim_{T\to\infty}\int_0^T E_n(t)E_m(t)dt=\frac{1}{2}E_{on}^2\ (n=m)\ or\frac{1}{2}E_{on}E_{om}\cos[\delta] \tag{11}$$

applying equation 10 to equation 9 and multiplying both sides of the equation by $4E_{ox}^2E_{oy}^2$ would yield:

$$2E_{ox}^2E_{oy}^2+2E_{ox}^2E_{oy}^2-\left(2E_{ox}E_{oy}\cos[\delta]\right)^2=\left(2\,E_{ox}E_{oy}\sin[\delta]\right)^2 \tag{12}$$

we explicitly keep the first two portions ($2E_{ox}^2E_{oy}^2$) in equation 12 separate, as adding and subtracting $E_{ox}^4+E_{oy}^4$ from the left side of equation 12 allows us to utilize the difference of perfect square rules (notably: $[A^2+B^2]^2=A^4+2A^2B^2+B^4$ and $[A^2-B^2]^2=-[-A^4+2A^2B^2-B^4]$). After adding and subtracting and using the difference of perfect square rules, we arrive at the following:

$$\left(E_{ox}^2+E_{oy}^2\right)^2-\left(E_{ox}^2-E_{oy}^2\right)^2-\left(2E_{ox}E_{oy}\cos[\delta]\right)^2=\left(2E_{ox}E_{oy}\sin[\delta]\right)^2. \tag{13}$$

We have finally arrived at the aptly named Stokes parameters of polarization. In equation 13, we write each term as follows:

$$S_0=E_{ox}^2+E_{oy}^2 \tag{14a}$$

$$S_1=E_{ox}^2-E_{oy}^2 \tag{14b}$$

$$S_2=2E_{ox}E_{oy}\cos[\delta] \tag{14c}$$

$$S_3=2E_{ox}E_{oy}\sin[\delta] \tag{14d}$$

These four equations are known as the Stokes parameters of polarization for plane wave oscillations [1, 2, 10]. For simplicity, we can re-write equation 13 using these parameters as follows:

$$S_0^2 = S_1^2 + S_2^2 + S_3^2. \tag{15}$$

These parameters determine the total intensity of a given source as well as its polarization state. Specifically, the total intensity of the light (I) is given by S_0 (which must be positive), while S_1 represents the intensity of horizontal / vertical polarization (positive and negative values respectively), S_2 represents the intensity of positive or negative 45º polarization (positive and negative values respectively), and S_3 represents the intensity of right or left circular polarization (positive and negative values respectively). All emitted light does not need to be polarized. Additionally, neighboring emitting sources can provide "competing" polarization parameters, which could interfere. To account for this Equation 15 is rewritten to be:

$$S_0^2 \geq S_1^2 + S_2^2 + S_3^2 \tag{16}$$

Chapter 4 will discuss this in greater detail. It is also noteworthy that, because these parameters are derived from the polarization ellipse, one can use them to obtain parameters such as the ellipticity and orientation angle from an emitting source, however we will not explore this further in this document.

The four stokes parameters by themselves are an interesting theoretical view of polarized light, however measuring them requires more mathematical manipulation. To begin, we start by forming the so called "Stokes vector:"

$$\vec{S} = \begin{pmatrix} S_0 \\ S_1 \\ S_2 \\ S_3 \end{pmatrix}. \tag{17}$$

Doing so allows us to create 4x4 matrices to describe optical elements such as polarizers and waveplates. Through matrix multiplication, these matrices can be used to interact with an incident beam, characterized by its Stokes vector and produce an outgoing beam, again described by its own Stokes vector. Specifically, if we consider an optical wave incident on some optical element, we can determine how the outgoing beam is related to the incident beam through a linear combination of all the initial

Stokes parameters and the matrix elements of the optical element. In matrix multiplication form, this would be expressed as:

$$\begin{pmatrix} S_0' \\ S_1' \\ S_2' \\ S_3' \end{pmatrix} = \begin{pmatrix} m_{00} & m_{01} & m_{02} & m_{03} \\ m_{10} & m_{11} & m_{12} & m_{13} \\ m_{20} & m_{21} & m_{22} & m_{32} \\ m_{30} & m_{31} & m_{32} & m_{33} \end{pmatrix} \begin{pmatrix} S_0 \\ S_1 \\ S_2 \\ S_3 \end{pmatrix}. \tag{18}$$

As a proof of concept, consider a beam of randomly polarized light traveling in the z-direction interacting with a horizontal linear polarizer (its transmission axis aligned with the x-axis). One expects the outgoing beam to be polarized in only the x-direction, meaning the only Stokes parameters present after interacting with the polarizer should be S_0, and S_1 (positive because the beam is aligning with the x-axis). Additionally, we include the factor $p^2$to account for attenuation of the beams intensity (p is squared because the intensity is given by the electric field squared). This polarizer be described in matrix element form by setting all m_{ij} matrix elements zero save the four in the top left quadrant. Specifically, m_{00}, m_{01}, m_{10}, and m_{11} which are all set to 1. The result would be as follows:

$$M_{horiz} = \frac{p^2}{2} \begin{pmatrix} 1 & 1 & 0 & 0 \\ 1 & 1 & 0 & 0 \\ 0 & 0 & 0 & 0 \\ 0 & 0 & 0 & 0 \end{pmatrix}. \tag{19}$$

For a perfect polarizer (complete transmission for polarization in line with the transmission axis), we set the attenuation factor p to 1:

$$M_{horiz} = \frac{1}{2} \begin{pmatrix} 1 & 1 & 0 & 0 \\ 1 & 1 & 0 & 0 \\ 0 & 0 & 0 & 0 \\ 0 & 0 & 0 & 0 \end{pmatrix} \tag{20}$$

Following matrix multiplication of the proposed random incident Stokes vector and this horizontally aligned linear polarizer, one can readily realize that the outgoing beam will contain only S_0, and $+S_1$, (S_2 and S_3 will be zero). This result is shown explicitly below:

$$\begin{pmatrix} S_0' \\ S_1' \\ S_2' \\ S_3' \end{pmatrix} = \frac{p^2}{2} \begin{pmatrix} 1 & 1 & 0 & 0 \\ 1 & 1 & 0 & 0 \\ 0 & 0 & 0 & 0 \\ 0 & 0 & 0 & 0 \end{pmatrix} \begin{pmatrix} S_0 \\ S_1 \\ S_2 \\ S_3 \end{pmatrix}. \tag{21}$$

Following through we find:

$$S_0' = \frac{p^2}{2}(S_0 + S_1) \tag{22a}$$

$$S_1' = \frac{p^2}{2}(S_0 + S_1) \tag{22b}$$

$$S_2' = 0 \tag{22c}$$

$$S_3' = 0. \tag{22d}$$

Not surprisingly, we obtain the desired outgoing beams polarization state: horizontally polarized light (given by a positive S_0' and S_1' parameter). As stated earlier, it is possible to follow through with this analysis for various optical elements. Of use in this project is a horizontally aligned linear polarizer (shown above) and a rotatable quarter wave plate. The matrix element of the quarter wave plate is given below as a function of the angle made between its fast axis and the x-direction:

$$M_{QWP}(2\theta) = \frac{1}{2}\begin{pmatrix} 1 & 0 & 0 & 0 \\ 0 & cos^2 2\theta & sin2\theta cos^2 2\theta & -sin2\theta \\ 0 & sin2\theta cos2\theta & sin^2 2\theta & cos2\theta \\ 0 & sin2\theta & -cos2\theta & 0 \end{pmatrix}. \tag{23}$$

Alone, these elements react with an incident beam as expected; the linear polarizer will polarize the incident beam along its transmission axis (unless vertical light is incident). The quarter wave plate will produce elliptically or linearly polarized light or whatever state in between depending on the incident state. However, setting these two optical elements in order, particularly the quarter wave plate followed by the horizontally aligned linear polarizer, one can completely describe the polarization state of an incident beam through measurement of the intensity of the beam after interacting with both elements in order. A schematic of this setup is shown in Figure 2, the matrix multiplication of this process is:

$$\overrightarrow{S'} = M_{horiz} M_{QWP} \vec{S}. \tag{24}$$

Where $\vec{S}$ is the optical disturbance of interest (incident on the setup), M_{QWP} is the rotatable quarter wave plate which is followed by the horizontally aligned linear polarizer, M_{horiz}.

$$M_{QWP}(2\theta) = \frac{1}{2}\begin{pmatrix} 1 & 0 & 0 & 0 \\ 0 & cos^2 2\theta & sin2\theta cos^2 2\theta & -sin2\theta \\ 0 & sin2\theta cos2\theta & sin^2 2\theta & 0cos2\theta \\ 0 & sin2\theta & -cos2\theta & 0 \end{pmatrix} \qquad M_{horiz} = \frac{1}{2}\begin{pmatrix} 1 & 1 & 0 & 0 \\ 1 & 1 & 0 & 0 \\ 0 & 0 & 0 & 0 \\ 0 & 0 & 0 & 0 \end{pmatrix}$$

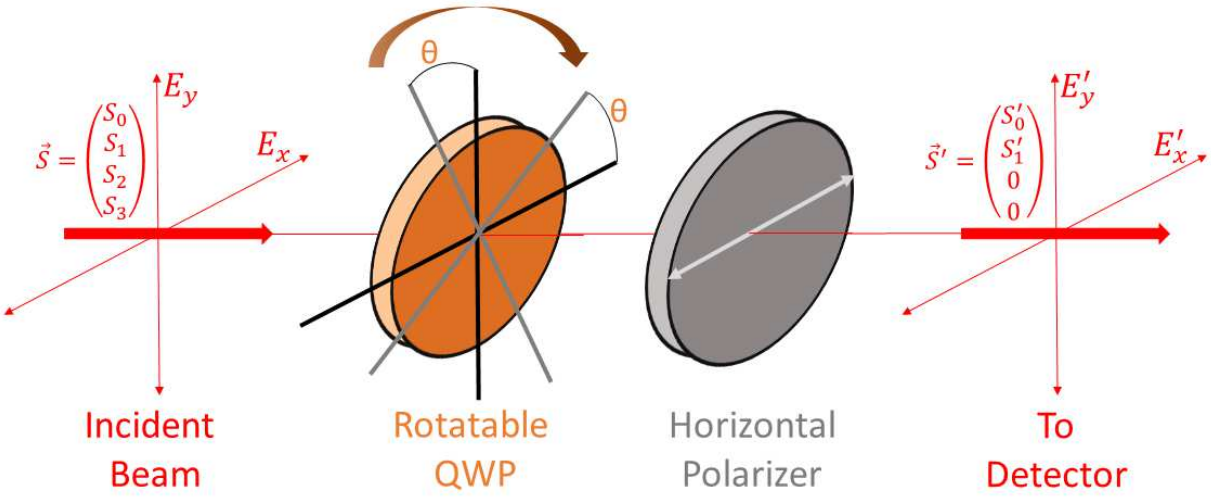

$$S'_0 = I(\theta) = \frac{1}{2}\left[\left(S_0 + \frac{S_1}{2}\right) + \frac{S_1}{2}cos4\theta + \frac{S_2}{2}sin4\theta - S_3 sin2\theta\right]$$

Figure 2. QWP-LP Setup

The result is the outgoing beam, determined by the incident beams interaction with the setup, shown above as $\overrightarrow{S'}$. Following through with the above suggested matrix multiplication, we arrive at:

$$\overrightarrow{S'} = \frac{1}{2}(S_0 + S_1 cos^2 2\theta + S_2 sin2\theta cos2\theta - S_3 sin2\theta)\begin{pmatrix} 1 \\ 1 \\ 0 \\ 0 \end{pmatrix}. \qquad (25)$$

The above expression is the crux of this dissertation, it allows us to fully describe the polarization state of an emitting source. This can be done through a measurement of the optical intensity of the beam after interacting with the quarter wave plate and the horizontal linear polarizer. Measurements can be conducted by whichever device is deemed most appropriate for the experiment. For this project, we used a CCD (Charged Coupled Device), specifications of which will be described later.

b. Experimental Setup

Below, Figure 3 shows a schematic diagram of the setup I built for this project, the full optical bench can be seen in Figure 4.

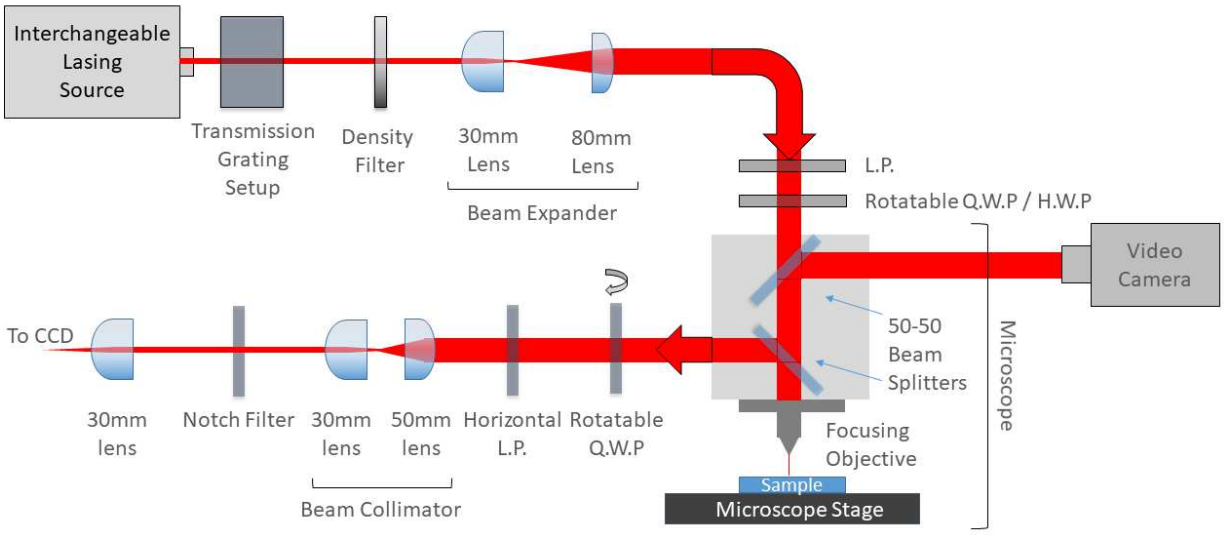

Figure 3. Schematic Diagram of Experimental Setup

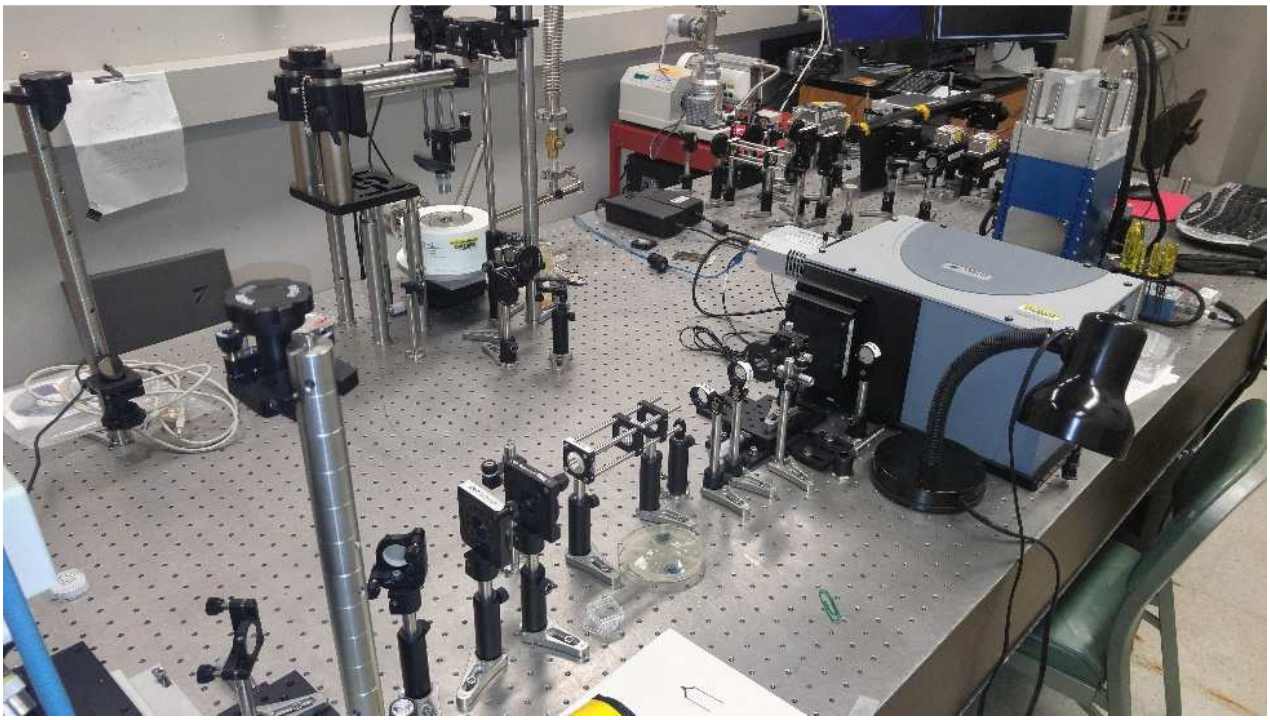

Figure 4. Experimental Apparatus Setup

Our experiment employs the use of multiple, interchangeable lasing sources (see Figure 5. Laser Selection and Monochrometer below) which, upon selection, passes through a transmission grating setup that serves as a single axis monochromator (see Figure 6 below).

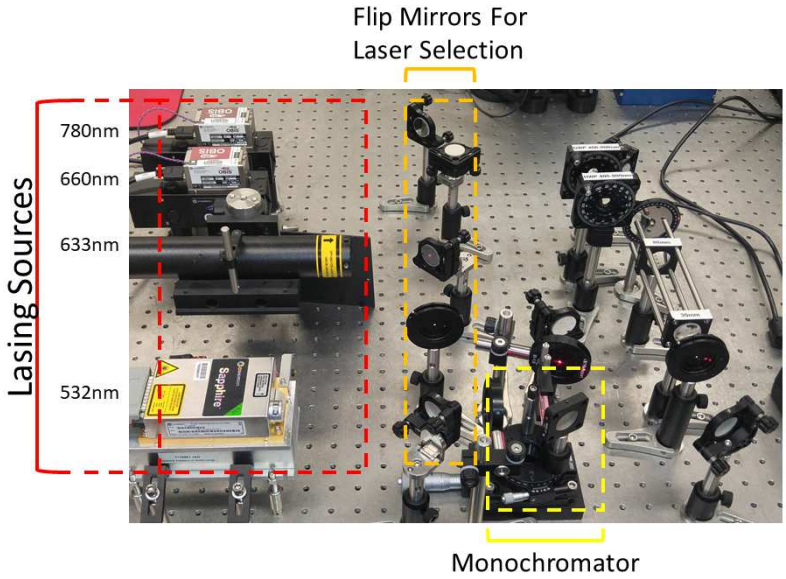

Figure 5. Laser Selection and Monochrometer

The table currently has four lasing sources which produce vertically polarized emission with the following wavelengths: 532nm, 633nm, 660nm and 785nm, each source is labeled in Figure 5. Laser Selection and Monochrometer above. Selecting a specific laser requires flipping mirrors up or down depending on desired source. Once the source is selected and the proper mirrors flipped, the beam then passes through a rotatable monochromator which is also labeled in Figure 5, a schematic diagram of this monochromator can be found in below Figure 6.

The design of this custom-built monochromator is based on standard transmission diffraction grating principles. It can be shown, for a standard transmission grating that the angle of incidence (θ_i) and resulting diffraction angle (θ_m), can be related to the interline spacing of the transmission grating (d), and the wavelength of incident light (λ_i) by [3, 4]:

$$d(\sin(\theta_i) + \sin(\theta_m)) = m\lambda \tag{26}$$

Here, m is an integer number and denotes the m^{th} order transmission. By passing our selected lasing

source through this setup, and selecting the first order transmission ($m = 1$), we can effectively filter out higher order wavelengths produced by the lasing sources, subsequently ensuring a more stable excitation. Reflecting this first order transmission off a mirror at an angle ϕ to the transmission grating then allows us to collect the beam later in the setup (the collection mirror can be seen in Figure 5). If we select the condition where the incident and transmission angle are the same, it can be shown that the angle β depicted in the schematic diagram is given by [3, 4]:

$$\beta = 2\phi - \theta \tag{27}$$

It should be apparent that this setup is only viable for one wavelength (λ). However, if the angle between the transmission grating and collection mirror is kept constant; and the entire apparatus is placed on a rotatable stage, the user can turn the stage to ensure the incident angle (θ_i) and the diffraction angle (θ_m), are equal. This allows us to maintain the condition for equation 27. Doing so, the operator ensures that, for any given wavelength, all lasing sources are produced parallel to each other. The only issue is, by rotating the apparatus, the translational position of the outgoing beam (λ_o) in is changed. We account for this by placing this rotating setup on a translational stage, now all wavelengths can be sent along the same path, and subsequently further into the full apparatus shown in Figure 4 and the schematic in Figure 3.

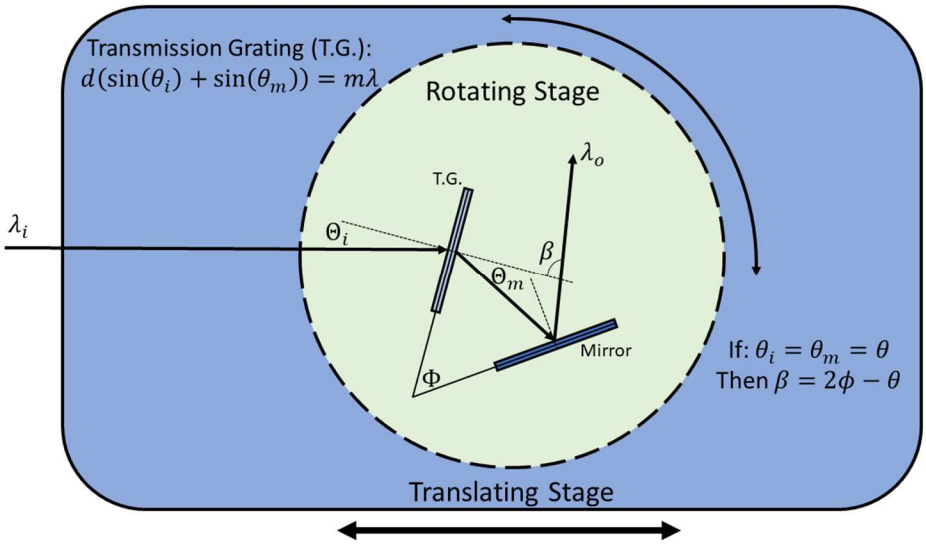

Figure 6. Schematic Diagram of Monochromator

After sending the beam through the monochromator, it then passes through a Thorlabs NDC-50C-4M density filter so the intensity can be attenuated as necessary. The laser beam is then expanded via a 30mm to 80mm lens system to ease alignment and better focus the beam when sent through our focusing objective. This beam can also be sent through a linear polarizer and / or quarter wave plate to ensure complete polarization or change the polarization state of the beam as necessary. This beam is then sent through an infinity corrected objective which focuses the beam on the sample. The beams reflection and any induced photo emission is collected back through the objective and split, a portion sent to a digital camera to acquire photos or video for focusing and alignment purposes. The other path is sent through the quarter waveplate – linear polarizer setup described within section 2a to relate the total emission intensity to the Stokes parameters of polarized emission. Because the photo luminescent emission can be across many wavelengths, we utilize a Thorlabs AQWP05M-600 achromatic quarter wave plate. The analyzed beam is then sent through a 50mm to 30mm beam condenser, which helps ensure the outgoing signal is collimated as it makes its way to the detector. The beam then passes through a notch filter, which we use to attenuate the exciting sources signal (more on this below). This light then passes through a 30mm focusing lens before passing into our spectroscope and detector.

Measurements are conducted using an Andor iDus 401 series model DV401A CCD and Shamrock model 303i spectroscope. This spectroscope allows for various reflective gratings, for this project, a 300 line per millimeter and 600 blaze grating was chosen, as it is best suited for optical spectra from the mid to upper wavelengths of visible light (500-900nm). The CCD and spectroscope are controlled via Andor Solis computer interface software. As mentioned above, a notch filter is in line before reaching the spectroscope. The notch filter serves to attenuate the exciting laser lines signal, else the CCD would over saturate, and no signal could be attained.

Stokes measurements are taken after rotating the quarter wave plate of the stokes setup. For completeness, measurements were taken by rotating the quarter waveplate by 10-degree increments, 36 times (for a complete rotation). Each measurement was taken and saved separately. Saved files were then processed and analyzed though the stokes formalism. This was accomplished through a code / script

written in MATLAB, which output the stokes parameters for polarized emission as a function of wavelength, allowing us to view polarization dependent optical spectra. This data could then be input into Origin for graphing and analysis. For reference, a typical fitting at a single wavelength is shown below in Figure 7. Fitting to the Stokes Formalism

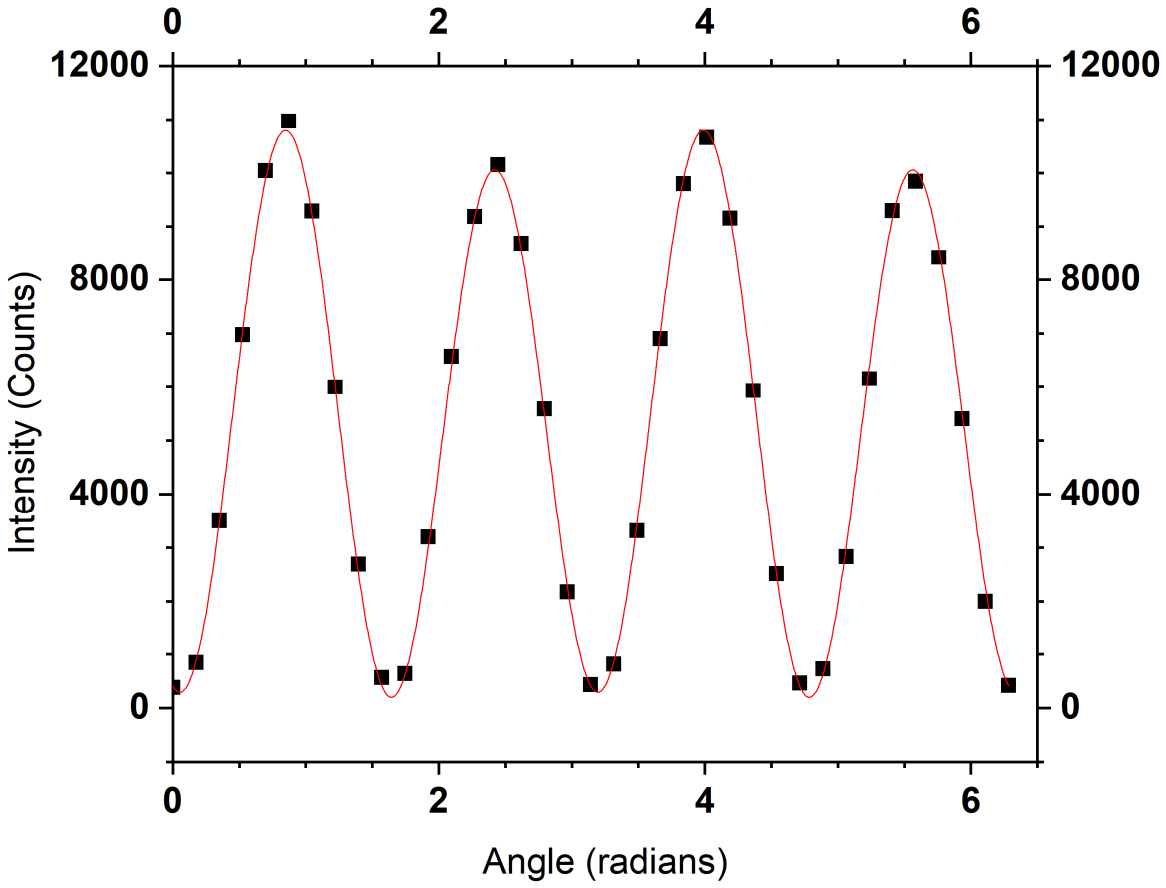

Figure 7. Fitting to the Stokes Formalism

Utilizing the MATLAB code as suggested to build a spectrum, fits such as the one shown in Figure 7 are used to acquire the stokes parameters of polarization at each wavelength, producing a polarization spectra. The light analyzed in Figure 7 was vertically polarized light, therefore we expect S_1 to present as a negative value, equal and opposite to S_0. S_2 and S_3 should be zero. The spectra associated with the fit in Figure 7 is shown below in Figure 8, where we indeed see that we have vertically polarized emission. The non-zero values of S_2 and S_3 can be attributed to reflections, and effects by optical elements, but are however essentially negligible, confirming that we have vertically polarized light.

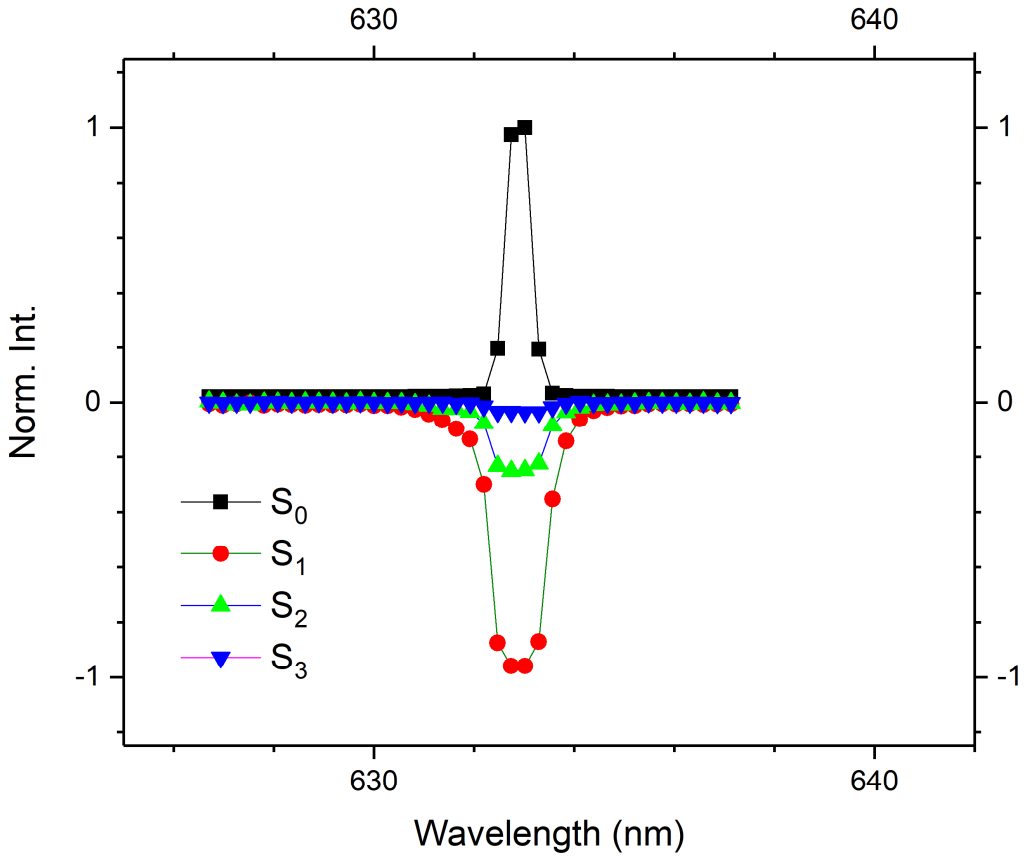

Figure 8. Proof of Stokes Measurement Concept

3. PHOTOLUMINESENCE AND POLYMERS – AN INTRODUCTION

a. Principles of Photoluminescence in Molecules

Luminescence has been the crux of research surrounding the study of materials for centuries [1, 2, 6, 11]. The phenomenon as a whole is best described as the spontaneous emission of electronic radiation from an excited species. The exciting source may induce an electronic state transition, or a vibrational mode variation within the species (among others); however the main outcome is the same: the excited species is now out of thermal equilibrium with its surroundings [6, 11]. A luminescent process is categorized by the way in which this excitation is prompted; for example, bioluminescence is spontaneous emission of light following chemical reactions within an organism (for example in oceanic algae), whereas electroluminescence is the result of electric field variation through a material (seen in fluorescent light bulbs) [6, 11].

This brings us to photoluminescence (PL), which can be understood as the spontaneous emission of electronic radiation following the interaction of a sample with a light source (the absorption of light by the species). The schematic diagram in Figure 9. General PL Schematic Diagram is shown to describe the general spontaneous absorption and emission process in materials such as molecules, polymers or direct band-gap semi-conducting materials [3, 5, 6, 11]. In molecules, the main components of the process include the absorption of an exciting wavelength λ (the source) with sufficient energy to bring an electron from the Highest Occupied Molecular Orbital (HOMO) to the Lowest Unoccupied Molecular Orbital (LUMO) of a material (in solid state materials these are replaced by the valance and conduction bands, and are continuums of electronic states), creating an electron – hole pair or exciton. The energy difference (or gap) from the HOMO to LUMO is determined by the orbital overlap in the molecule (in solid state materials, the valance and conduction bands energy gap is determined by the atomic configuration, among

other things) [5, 6, 11]. After the absorption and excitation process, the wavy line in Figure 9. General PL Schematic Diagram shows how the electron, now in the LUMO, can vibrationally (non-radiatively) relax to the bottom, or lowest energy of the LUMO state. Once at the bottom of the band the electron can now spontaneously recombine with the HOMO, in doing so producing EM radiation. The resulting PL is directly related to the energy gap between the HOMO and LUMO of the molecule, with $E = h\nu_{em} + heat$ dictating the frequency (ν_{em}) of the resulting photo-emission from an energy difference E (h is planks constant), *"heat"* is included to consider other forms of energy conversion during the process. In molecules, the timeframe from spontaneous absorption to recombination can be anywhere from the order of femto- to nano- seconds and is strongly dependent on material properties [3, 5, 6, 11]. Additionally, other processes such as inter-system crossing and phosphorescence can occur, however they won't be the focus of this discussion.

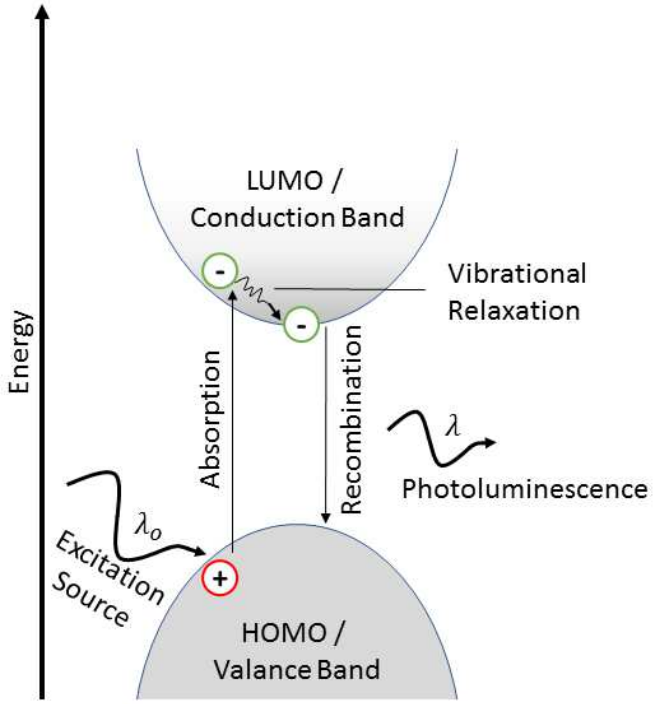

Figure 9. General PL Schematic Diagram

For Molecules, the PL schematic diagram in Figure 9 is a bit misleading as it assumes a continuum of states within each band (a good approximation for solid state materials). Instead, it is more

prudent to consider a Jablonski diagram, which considers the ground and excited states of the molecule and their subsequent vibrational levels through the lens of the molecular orbital theory (which is a particular implementation of the Schrodinger equation). The traditional diagram allows for singlet and triplet states (determined by the total spin quantum number equaling one or three respectively) [39, 40]. Direct excitation from the singlet ground state to the triplet excited state is generally forbidden. However, through spin-orbit coupling, it is possible for states of different spin multiplicities to interact. This leads to a slight variation of the wavefunction of one spin multiplicity state to contain a small contribution from the other. The resulting interaction / possible transition from the excited singlet state to the triplet state is called intersystem crossing, which can result in phosphorescence (the recombination to the ground state from the excited triplet state). A detailed discussion of accessing each state requires group theory considerations, and given the small contribution in our systems we consider them to be negligible, and therefore choose to consider only singlet-singlet transitions for this discussion [6, 11].

Continuing, a version of a Jablonski diagram is shown in Figure 10. Here, we see an analogous situation to Figure 9, however instead of a continuum of vibrational states, there are specific energy levels denoted by A_0, A_1, and T_1 for the ground state, the first excited state and the first triplet state of the molecule (with included discrete vibrational energy levels for each state). It should be noted that higher electronic energy levels (A_2, A_3, T_2, T_3 etc.) and their vibrational levels are permitted, however for ease of discussion they are excluded. Triplet states are only accessed through intersystem crossing from the first excited state to the triplet state. Again, for a particular molecule, the values of the energy levels and their vibrational levels are determined through molecular orbital theory. In this case, we consider A_0 to be the HOMO and A_1 the LUMO [6, 39]. As with Figure 9. General PL Schematic Diagram, Figure 10. Jablonski Diagram. depicts the spontaneous excitation of an electron from the HOMO to the LUMO state. This electron can then non-radiatively decay to the lowest level of the excited state and triplet state (shown as squiggly arrows), and finally radiatively decay back to the ground state, called photoluminescence when de-excitation is from the first excited singlet state and phosphorescence when

from the first excited singlet state and phosphorescence when from the first excited triplet state.

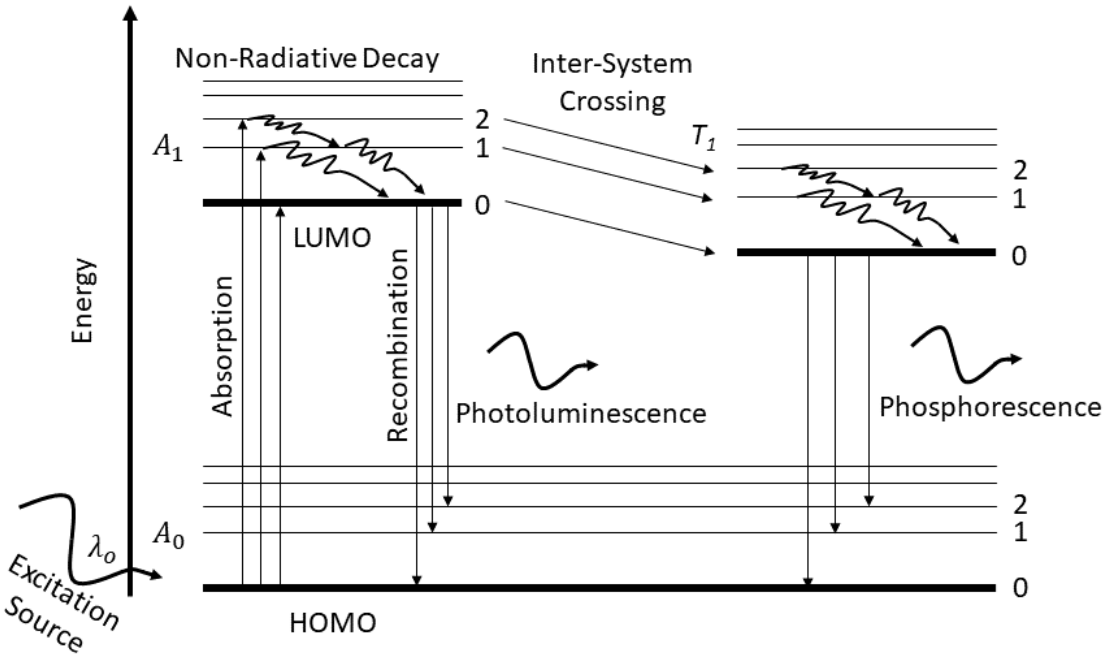

Figure 10. Jablonski Diagram.

Notice, that there are multiple possible absorption lines leading from the lowest vibrational level of the ground state to various levels of the excited state, in practice these are denoted as $0 \rightarrow n$ absorption transitions, with n being the nth vibrational mode (starting at zero). Upon reaching the nth vibrational energy level of the excited state, non-radiative decay brings the exciton the bottom of the LUMO state. From here, recombination can occur to any of the ground state vibrational levels, denoted as $0 \rightarrow n$ emission transitions, with n being the nth vibrational mode of the ground state (starting at zero). One can plot the absorption and subsequent emission intensities as a function of wavelength, a schematic of which along with another visualization of excitation – de-excitation (the Franck-Condon progression), is given in Figure 11 below.

The exact vertical line values of the $0 \rightarrow n$ absorption (emission) would be the exact values expected for a vapor of a given molecule. When in solution or film, broadening can occur (especially with increasing temperature), which shows as the more gaussian like lines surrounding direct vibrational level transitions. The absorption and emission spectra tend to follow the "mirror image" rule, where they are

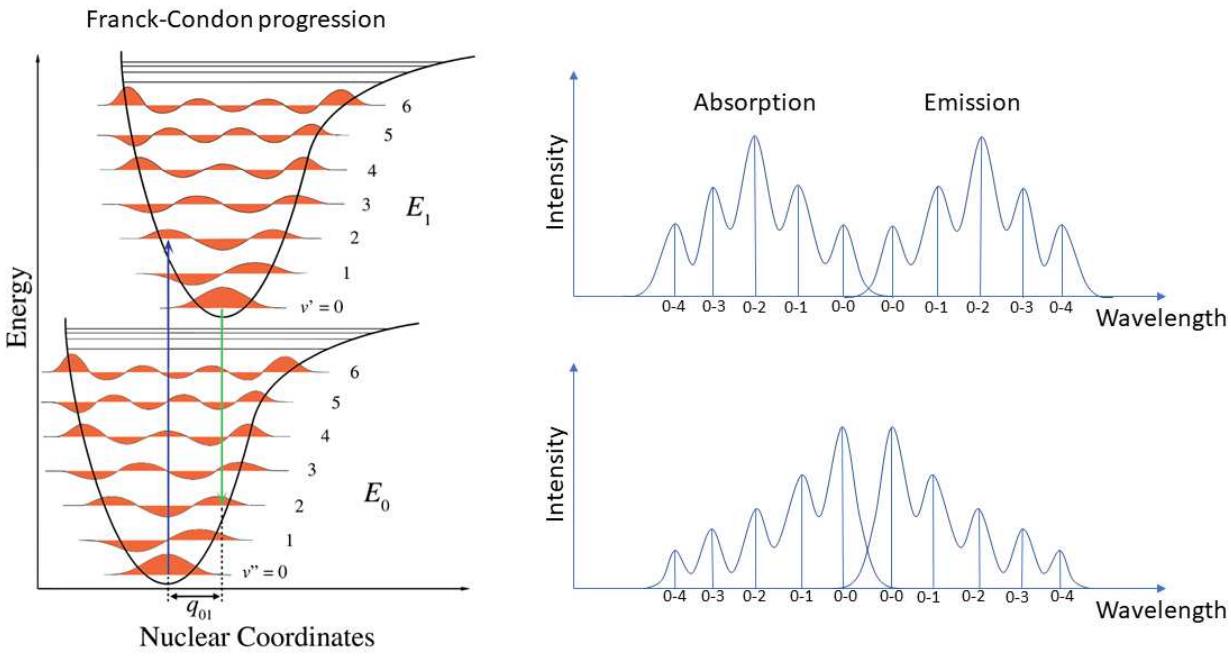

Figure 11. Absorption and Emission Schematic

just that, a mirror image of each other, this isn't however a hard and fast rule as is the case with some polymers and other systems. The difference in peak positions from absorption to emission is referred to as a Stokes shift, which could be a result of heat loss, for example (hence why $E = h\nu + heat$ earlier) [6, 11]. The difference in shape from the top schematic plot to the bottom is explained through the Born-Oppenheimer approximation and the Frank-Condon principle, which considers the wavefunction of the electrons with respect to electronic variables and nuclear variables. The two in combination assumes that the movement of electrons is paramount to that of nuclear positions, and that the molecular orbital positions with respect to nuclear position may cause the HOMO and LUMO to be at different radial positions (from the nucleus). Transitions will therefore more readily occur between wave functions for which the peak positions between two given vibrational energy levels (from the LUMO to the HOMO) are aligned, meaning absorption and subsequent emission will be more likely in wave functions with better peak alignment. This results in unequally expressed transition intensities [6, 9, 11].

The electronic transitions as a result of absorption described in molecules can occur following excitation from sources in the UV, visible and near-infrared (NIR) spectral regions (see Figure 1) [6, 11].

The exact value of the energy gap (and therefore the spectral region required to cause spontaneous excitation) is determined by the bond structure of the molecule in question [6, 11]. Of particular interest for this report (and specifically the polymers P3HT and P(NDI2OD-T2) is the $\pi \rightarrow \pi^*$ transition; the π-orbital being formed by two p atomic orbitals overlapping, and the π^* being the anti-bonding orbital from the same p atomic orbital overlap. These orbitals are the HOMO and LUMO respectively in the case of the $\pi \rightarrow \pi^*$ transition (however the terms are general and apply to all such molecular systems).

It is found that in molecules with a particular transition moment; that is, a directional dependence for spontaneous absorption formed through orbital overlap, light polarization can play a role in the excitation and subsequent emission process. Such is the case for π-orbitals formed in aromatic rings, whose polymer backbone and subsequent aggregation play a key role in light absorption. This polarization dependence will also be important in P3HT / P(NDI2OD-T2) although because they're polymers, the polymer backbone will be of additional importance. In such molecules, the fluorophores (the species which can be excited) with their axis in the same orientation as linear polarized light are most readily excited, while those off axis are less accessible. This means any such absorption, $A_0 \rightarrow A_1, A_0 \rightarrow A_2$, etc. whose spatial orientation is in partial alignment with the linear polarized excitation can be accessed. The probability of excitation is given by the square of the dot product of the transition moment $\vec{M}$ with the electric field vector of the excitation source $\vec{E}$: $\left(\vec{M} \cdot \vec{E}\right)^2$, in other words, it follows a $\cos^2 \theta$ dependence, where θ is the angle between $\vec{M}$ and $\vec{E}$. The subsequent emission however does not depend on the incident sources polarization, the outgoing emission will be polarized along the transitions axis once the state is accessed [6, 11, 37, 41].

b. Conjugated Polymers P3HT and NDI

Polymeric semiconducting materials have rapidly developed over the past few decades as a direct result of their ability to serve as solution processable, corrosion resistant and flexible electronic devices such as light-emitting diodes, solar cells, field-effect transistors and sensors [15, 17, 20, 34, 36, 38, 42-45]. Poly{[**N**,**N9**-bis(2-octyldodecyl)-naphthalene-1,4,5,8-bis(dicarboximide)-2,6-diyl]-alt-5,5**9**-(2,2**9**-

bithiophene)} or P(NDI2OD-T2) has emerged as a leading n-type polymer due to its high electron mobility and stability under ambient conditions (it's chemical diagram is given below in Figure 12. P(NDI2OD-T2) and P3HT chemical diagrams) [14, 17, 33, 35, 38, 43-51]. The bithiophene unit is an electron donor and the naphthalene diimide unit is an electron acceptor. The resulting band gap is approximately ~1.5 eV. Early structure-property measurements of P(NDI2OD-T2) films were unable to recover high electron mobility values obtained from FET measurements with an unexpected out-of-plane π-π stacking observed in x-ray diffraction experiments. Using GIWAXS Rivany et al. showed that the P(NDI2OD-T2) chains pack in crystalline lamellae with the donor-acceptor moieties in a "face-on" orientation (i.e., parallel to the substrate) when spin-coated and annealed below 300^{o}C [35]. However, when the films were annealed to the melting point and slowly cooled, the donor-acceptor groups change into an "edge-on" (i.e., perpendicular to the substrate). Subsequent x-ray diffraction and electron/optical microscopy studies confirmed the change in orientation. Using NEXAFS, Schuettfort et al. discovered that the surface layers of P(NDI2OD-T2) retain a face-on orientation even after thermal annealing, which is the transport layer in an FET [45]. These initial studies motivated many more structure-property measurements. In particular, the influence of polymer molecular weight/polydispersity, solvent processing, and annealing have been studied in detail [37, 38].

A more detailed molecular view of the polymer orientation in the solid state has emerged from IR spectroscopy. Using polarized transmission and reflection-absorption infrared spectroscopy (RAIRS), which follow rigorous dipole selection rules, the orientation of the naphthalene diimide and bithiophene groups with respect to each other (and the substrate) have been quantified [44, 46]. Giussani et al. used reflection-absorption infrared spectroscopy to determine that the bithiophene units lie parallel to the substrate and the naphthalene diimide units are tilted out of plane, which yields an approximate dihedral angle of 38^{o} [44]. Anton et al. were able to refine the orientation of the NDI and bithiophene units by measuring the polarization and angle-dependent RAIRS spectra, which allows for complete determination of the absorbance tensor. They also studied the thickness dependence (150 nm vs. 1.5 micron) and found the out-of-plane order is almost unchanged with increasing thickness, while the in-plane order decreases.

In a detailed study by Steyrleuthner et al. the influence of solvent on P(NDI2OD-T2) aggregation, both in the solution and solid-state, was elucidated. Using a combination of UV-vis, photoluminescence, NMR and analytical centrifugation several characteristics of aggregates were identified [51]. First, in "good" solvents (e.g. chloronapthalene) the low energy absorption peak is near 635 nm and the emission peak appears near 800 nm. In contrast, in "poor" solvents (e.g. toluene) the low energy absorption peak appears near 700 nm and the emission peak wavelength is near 850 nm. The observed solvatochroism was supported by DFT calculations that indicate the red-shift in the absorption spectra was mainly due to chain aggregation. Second, the observed photophysical properties did not depend significantly on polymer concentration (i.e. 0.01 mg/mL to 1 mg/mL). A careful analysis of the emission band shape, along with time-resolved photoluminescence measurements, revealed three characteristic spectral regions: in solution (cast films) emission from 710-730 (690-700) nm was assigned to intrachain excitons, while emission from 770- 790 (770-800) nm and 840-860 (850-900) was assigned to aggregate "I" and "II", respectively.

Poly(3-hexylthiophene), or P3HT is another such conjugated polymer system that has received remarkable consideration in the search for polymer based semi-conducting devices. P3HT stood out as a leading champion among p-type conjugated polymers due to its ease of synthesis, the overall stability offered by its polythiophene unit, as well as its ability to be tuned according to application requirements (the 3-Hexylthiophene unit presents the possibility to tune the regioregularity of the resulting polymer) [9, 16, 21, 33, 52, 53].

Early, unsubstituted synthesis of polythiophenes was reported in 1980 [16, 54]. 3-alkylthiophenes (and therefore P3HT) are asymmetric monomers, therefore three separate configurations exist when connecting thiophene rings between the 2- and 5-: a 2-2' coupling (head to head [HH]), 2-5' coupling (head to tail [HT]), or 5-5' coupling (tail to tail [TT]). A mixture of these coupling schemes is referred to as regioirregular or regiorandom [16]. In regioirregular samples, HH coupling is unfavorable; a result of the thiophene units twisting from planarity, doing so drastically decreasing the conjugation length. Conversely, completely regioregular samples favor HT schema, allowing the polymer to present a more planar conformation. The first report of regioregular P3HT was reported McCullough and Lowe

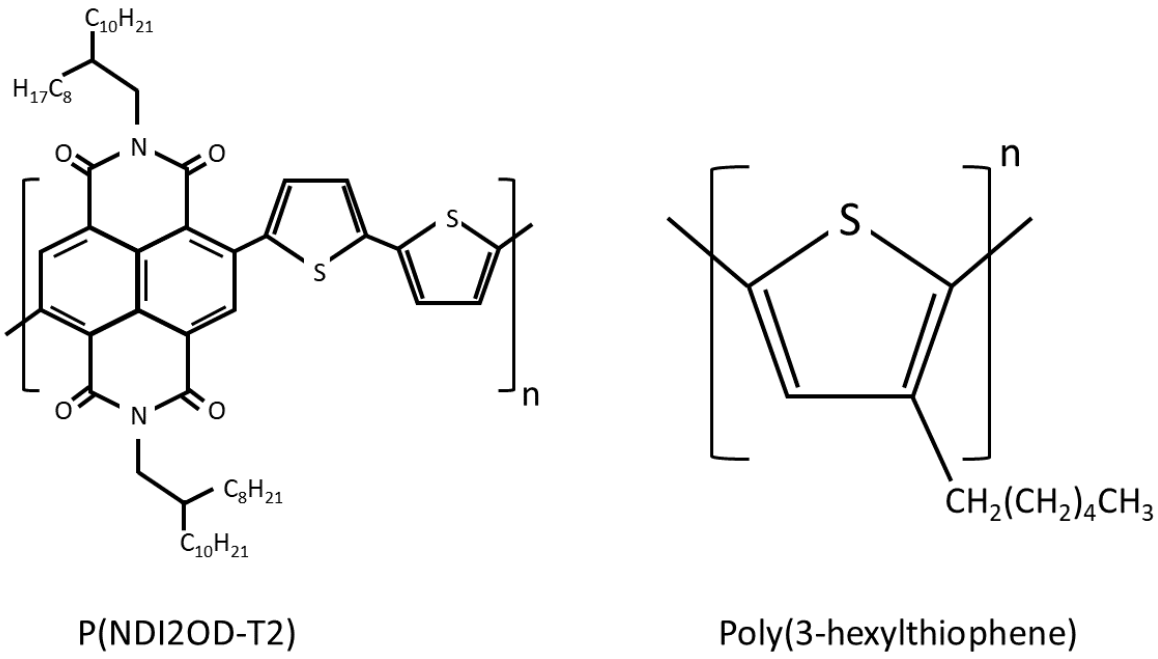

Figure 12. P(NDI2OD-T2) and P3HT chemical diagrams

[16, 55, 56]. This formation is preferable for device application, as charge transport is more readily realized through long range π-conjugation.

As stated, P3HT p-type semiconducting π-conjugated polymer. Through electrochemical measurements, regiorecular P3HT was found to have HOMO and LUMO energy levels of approximately -5.1 eV and -2.4 eV respectively [16, 57, 58] resulting in a band gap of approximately 2.7eV.

Absorption measurements of P3HT in solution present as a single broad peak without abnormal features. This is attributed to the coiled conformation of isolated chains [16, 59]. When comparing the absorption and fluorescence spectra of regioregular to regioirrgular P3HT solutions in chloroform, one observes a blue shift of the peak positions. This is a result of a decrease in the conjugation length, which is a result of polymer backbone twisting, driven by the spatial arrangement of atoms [16, 30, 60-62]. The conjugation length of regioregular P3HT is additionally affected by the polymers chain length.

While conjugated polymers such as P3HT generally favor 1-dimensional nano-rod like formations; strong π-π interactions perpendicular to the polymeric backbone, as well as hydrophobic tendencies of side chain units, can result in aggregation in P3HT [16, 30, 63]. The first report of P3HT

crystallization due to a poor solvent was presented by Ihn et. al. [16, 63]. Through AFM, TEM and X-ray analysis it was found that P3HT nano-fibrils would pack normal to the polymer backbone (known as π-stacking), while the alkyl side-chains oriented perpendicular to the substrate (known as an edge-on orientation). Since this initial work, much research has been conducted to understand the formation, performance, and application of such aggregation [16, 27, 28, 30, 31, 63-65].

When cast from solution, is has been shown that P3HT films can exhibit both H-, J-, and HJ- like aggregate formation [16, 22, 27, 28, 30, 31, 53, 63, 65, 66]. However, it is generally accepted that H- and HJ- like behavior is dominate. A series of work by Spano et. al. has provided; through quantum mechanical calculation and modeling, a method by which one can determine a series of characteristic parameters such as the spatial correlation length, coherence length, and coherence number, based upon the ratio of vibrionic peaks from either H- or J- like formations in absorption and fluorescence measurements [9, 24-31]. It is generally accepted that H- like peaks present as a series of 3 peaks, representing the 0-0, 0-1, and 0-2 transitions, with approximate peak positions 685nm (1.81eV), 751nm (1.65eV), and 838nm (1.48eV) respectively. For J- like peaks, the positions of the 0-0 and 0-1 transitions are located at approximately 635nm (1.95eV) and 695nm (1.78eV) respectively. These peaks are expected for low temperature measurements (~10K) and the peak positions of H- (J-) like formations are expected to blue- (red-) shift with increasing temperature [9, 24-31]. The differences in these peak positions are determined by variations in the selection rules dictating H- and J- aggregate formation, which will be discussed further in section c of this chapter.

c. Polymer Aggregation (the H-, J-, and HJ- model)

In order to begin talking about aggregate behavior in crystalline organic materials (organic polymer aggregates), we should first go back and discuss in more detail the quantum mechanical framework of energy transitions in molecules (and polymers). We therefore begin by establishing the Hamiltonian for N identical molecules, the i^{th} electrostatically coupled to neighbor j via potential V_{ij}, with $(i = 1, 2, \dots, N)$. Doing so, we can write the following Hamiltonian for the polymer in question [9, 67]:

$$H = \sum_{i=1}^{N} (H_i + \Delta H_i) + \frac{1}{2} \sum_{\substack{i,j=1 \\ i \neq j}}^{N} V_{ij} \tag{28}$$

Here, H_i is the Hamiltonian for each individual molecule while ΔH_i is a variation added to account for static and dynamic disorder between neighboring molecules. The ground state wavefunction for an electron associated with this molecular array Hamiltonian is then approximated as the product of all the individual wave function ψ_{i0} making the full ground state wave function:

$$\Psi_{Ground} = A \prod_{i=1}^{N} \psi_{i0} \tag{29}$$

Here, A is the antisymmetrization operator. This operator accounts for fermions within the wavefunction under the lens of the Pauli Principle. Essentially, it makes the wavefunctions of N of these identical fermions antisymmetric under any pairs coordinate exchange. Continuing, the excited state wavefunction of a produced exciton can be written as:

$$\Psi_{Excited} = \sum_{j=1}^{N} c_j \Psi_{jE} \tag{30}$$

c_j are coefficients obtained through application of the variational principle to the Schrodinger equation, and when dealing with local excitations (such as Frenkel excitons) the excited state wavefunction can be represented as:

$$\Psi_{j\,Excited} = \psi_j \prod_{\substack{i=1 \\ i \neq j}}^{N} \psi_{i0} \tag{31}$$

This form is utilized as Frenkel excitons are again local, meaning the excited molecule j remains coupled to the remaining $N - 1$ molecules in the ground state. It is important to note, that the consideration for these wavefunctions is for individual molecules, or simply put: don't consider the effect of the electrostatic interaction between molecules [9, 67].

The potential interaction between neighboring molecules V_{ij} prompts shifts in the ground state

energy (known as the gas to crystal shift) and causes shifts in the excited state energy when compared to non-interacting molecules. These shifts are found by finding the expectation value of the electrostatic interaction between molecules with the ground and excited state wavefunctions $D_{Ground} = \langle \Psi_{Ground} | \left(\frac{1}{2}\right) V_{ij} | \Psi_{Ground} \rangle$, and $D_{Excited} = \langle \Psi_{j\,Excited} | \left(\frac{1}{2}\right) V_{ij} | \Psi_{j\,Excited} \rangle$ respectively.

With all of this in mind, we can consider the energy levels for the molecular chain to be of the form:

$$E = E_j + \Delta D + 2J_0 \cos(ka)\,. \tag{32}$$

Here, E_j is the excitation energy when considering the non-interacting molecule, ΔD is the difference between the energy shift of the ground state to the excited state, and $2J_0 \cos(ka)$ is a periodic boundary condition; considering a to be the distance between nearest neighbors, and $k = 0, \pm\frac{2\pi}{Na}, \ldots, \pm\frac{\pi}{a}$. J_0 is the energy associated with the interaction between neighboring molecules (known as the resonance energy) and is given by $\langle \Psi_{jGround} | \left(\frac{1}{2}\right) V_{ij} | \Psi_{jGround} \rangle$. A bandwidth of $4J_0$ is expected when there are N coupled molecules form Frenkel exciton states (the specific type of excited state band). Momentum conservation drives the selection rules for this array, and requires that photoexcitation from source λ excites only the excitonic state with $k = \frac{2\pi}{\lambda}$. Because exciting wavelengths are much larger than the molecular spacing (and therefore lattice constant a above), only excitons at or near the bottom (top) of the exciton band can become populated following excitation. Depending on the molecular arrangement, these selection rules will result in differing shapes and ranges for photo-absorption and subsequent photo-emission [9, 67].

For our purposes, there are two particular arrangements (and subsequent selection rules) of heightened interest: H- and J- aggregates (and therefore HJ- aggregates). These aggregates types are of particular importance for P3HT and P(NID2OD-T2) as they tend to form in π-stacks. When these polymers arrange in a face-to-face like orientation, the stack is referred to as an H-aggregate. When they arrange head-to-tail, they are referred to as J-aggregates. An HJ-aggregate would therefore be a combination of the two. When we consider a linear array of molecules favoring nearest neighbor

interaction between neighboring molecules the sign of J_0 will dictate the type of aggregate formed. When J_0 is found to be greater than zero, the formation of H-aggregates is expected. For J_0 less than zero, J-aggregates are formed [9, 27, 30]. This is because sign of the coupling constant dictates the shape of the lowest vibrionic bands energy dispersion, and therefore creates particular selection rules for each type of aggregate [9, 27, 30]. Further discussion of H-, J- and HJ- aggregate behavior and modeling is found further in Paper 2, below.

PAPER 1: BROADBAND POLARIZED EMISSION FROM P(NDI2OD-T2)

a. Paper 1: Abstract

We investigate the photophysical properties of P(NDI2OD-T2) via absorbance and fluorescence spectroscopy, in association with an experimental approach named Stokes Spectroscopy, which provides valuable material information through the acquisition and analysis of the light's polarization degree. By changing the solvent type and by utilizing either solutions, thick, or thin films, it is possible to control the polarization degree as function of the wavelength for the emissions from the ICs and aggregates. We show that the polarization degree has great potential as a tool to access information related to morphology of the samples, by inferring about their microscopic structure. Moreover, the polarization degree spectra brings evidence that depolarization effects caused by energy and charge transfer mechanisms may be taking place. Our findings suggest P(NDI2OD-T2) polymers as excellent candidates for further advancing technologies that are based on polarized lights' detection and emission.

b. Paper 1: Introduction

The need for optical devices capable of emitting polarized light is fundamentally important in applied physics, with a potentially high impact on technologies from the optoelectronic industry, e.g. optical displays, data storage, information processing and others [12]. Over the past decades, the search for such polarized light emitters (PLEs) has gained momentum, pushing the development and manipulation of materials to produce desired polarization outcomes. Examples of PLEs include; liquid crystals doped with dye molecules [12, 68], quantum dot arrays [69], quantum dots dispersed in a GaAs-based chiral nanostructure [70], bundled multiwall carbon nanotubes [71], fluorescent polymers prepared via the Langmuir Blodgett technique [7, 72] and aggregated polymers in solution [23].

Semiconducting polymers have been considered as potential candidates for a variety of devices

including organic light-emitting diodes, solar cells, field-effect transistors, and sensors [15, 17, 20, 34, 36, 38, 42-45]. These materials have potential to be used as PLEs, and can be easily integrated in organic-based electronic technologies that have already been developed. The polymer P(NDI2OD-T2) or poly([**N**,**N9**-bis(2-octyldodecyl)-naphthalene-1,4,5,8-bis(dicarboximide)-2,6-diyl]-alt-5,5**9**-(2,2**9**-bithiophene)) has emerged as a leading n-type polymer due to its high electron mobility and stability under ambient conditions [14, 17, 33-35, 37, 38, 43-45, 48-50, 73]. The bithiophene unit is an electron donor and the naphthalene diimide unit is an electron acceptor, this combination leads to a low band gap (~1.5 eV). Here, we investigate the photophysical properties of P(NDI2OD-T2) via absorbance and fluorescence spectroscopy in a non-invasive and intuitive optics-related technique capable of providing valuable material information through the acquisition and analysis of polarized light emission [1, 10]. We use an extended configuration of the setup suggested in references [1, 10, 74-76] which replaces monochromatic linear polarizers and quarter wave plates by their achromatic counterparts and introduce computational methods for data processing. This arrangement allows us to map, simultaneously, the polarization of the emitted fluorescence through a broad spectral range, and allows us to determine the influence of different solvents and film thickness on the polarized emission throughout the whole spectral range of the fluorescence emitted by P(NDI2OD-T2) polymers.

c. Paper 1: Results and Discussion

Our experiment employs the use of a 633nm, 17mW linearly polarized He-Ne laser as an excitation source. The beam is sent through a linear polarizer to ensure complete polarization and then sent through a 100x / 0.9 N.A., infinity corrected objective which focuses the beam on the sample. The intensity of the beam incident to the sample was controlled by a density filter to avoid sample damage. The reflection of this beam is collected back through the objective and, before reaching the detector, passes through an achromatic quarter wave plate – linear polarizer apparatus used to acquire the Stokes parameters over a wide range of wavelengths. Signal detection is performed using an Andor iDus 401 series CCD; and Shamrock spectroscope, which utilizes a 300 lines-per-millimeter and 600 blaze grating. To conduct Stokes spectroscopy, the quarter wave plate and linear polarizer are set with their fast axis and

transmission axis in the horizontal direction. Spectra measurements are taken after rotating the quarter wave plate in increments of 10º, from zero to 360º. P(NDI2OD-T2) was purchased from polyera corporation and used without further purification. Films of P(NDI2OD-T2) were factored, dropping precursor solution prepared in three different solvents: Chloronaphthalene (CN), Dichlorobenzene (DCB) and Toluene.

The absorption spectra for solutions, spin-coated films and drop-casted films in different solvents is shown in Figure 13. P(NDI2OD-T2) Absorbance Comparison. The figure shows, from the left to right panel, the absorbance spectra for solution and films prepared with CN, DCB and Toluene, respectively (*the shaded curve, in the middle and right panel, refers to the absorbance of CN-solution, in which isolated chain (IC) is expected*). The CN-based solution displays the absorption curve centered about 610 nm, which is a fingerprint of IC absorption [37]. As the quality of the solvent decreases, the absorption peaks for aggregate I (Agg I) and aggregate II (Agg II) species are present [37]. For the "intermediate" solvent (DCB) and the "bad" solvent (Toluene) both Agg I (with absorption around 715 nm) and Agg II (with absorption around 815 nm) species seem to be present, although Agg I species seem to dominate. The colored stripes in Figure 1Figure 13 highlight the spectral region where the absorption for IC (green stripe), Agg I (blue stripe) and Agg II (red stripe) is expected to take place [34, 37, 38, 43]. The spectra also suggest that film formation enhances the aggregation process by favoring the formation of aggregates I and II. For solutions prepared in Toluene, the absorbance from the films are nearly identical to the solution absorbance, which leads us to the conclusion that, for this solvent, most of the aggregation occurs while in solution and the film formation no longer plays a major role in aggregate formation. Our observations are in accordance with Steyrleuthner et. al. [37], which suggested that the CN-based solution is comprised of mostly IC, the DCB-based solution seems to be composed of a balanced amount of IC and Agg I with a small contribution of Agg II, and the Toluene-based solution, when compared with the CN-based solution, seems to exhibit all three species. However, for the Toluene-based solution, Steyrleuthner et. al. [37] suggest that the Agg I species is totally converted into Agg II

species and, therefore, they attributed the absorption peak centered at approximately 715 nm to an Agg II vibronic progression that coincidently absorbs at the same wavelength as the Agg I, which indeed seems to be the case. The π-π* peak positions for CN, DCB and Toluene films redshift relative to the π-π* peak position for the CN solution (about 10 nm for CN drop-casted film and 20 nm for the other cases). This redshift is not a solvatochromatic shift, but instead, it is a signature of aggregation [37, 38, 43, 77]. It is important to address some aspects related to the film formation. *Our results show that the relation between a solvent's boiling point and thickness of the films are important variables in controlling the formation of aggregates*. The absorption curves for spin-coated films casted from different solutions look similar to each other. For the drop-cast films, with thicknesses that are at least one order of magnitude larger than those of the spin-coated films, the thickness seems to be playing a role together with the boiling point temperatures for the solvents. The boiling point temperatures are 110.6 ^{o}C for Toluene, 180.0 ^{o}C for DCB and 259.0 ^{o}C for CN. Specifically: with increased thickness, CN based films take longer to evaporate than DCB and Toluene, which is, in part, because of the difference in boiling point. As a result, different boiling points give more time for either IC maintenance (as it seems to be the case of CN-based films) or Agg I and II formation (as it seems to be the case of DCB and Toluene-based films).

To gain further insight on the films and solutions, we now look at the fluorescence (FL) spectra (see Figure 15 in the Supplementary Information) emitted by the samples under the Stokes Spectroscopy scope. To the best of the authors knowledge, the FL spectrum for P(NDI2OD-T2) has not been thoroughly explored yet. The Stokes Spectroscopy technique, which is based on the Stokes formalism for polarized light [1, 10], analyzes light by decomposing it into 4 wavelength-dependent parameters: $S_0(\lambda)$, which is proportional to the total intensity of the light; $S_1(\lambda)$, which describes the vertical/horizontal linear polarizations; $S_2(\lambda)$, which describes the ±45^{o} linear polarizations; and $S_3(\lambda)$ which represents the left/right circular polarizations. In theory, $S_0(\lambda) \geq \sqrt{S_1^2(\lambda) + S_2^2(\lambda) + S_3^2(\lambda)}$, where the equal sign stands for totally polarized light and the inequality sign stands for a mixing of polarized and unpolarized lights (in other words, partially polarized light). In this context it is possible to define the lights polarization

degree (PD) as, $PD(\lambda) = \sqrt{\left(\frac{S_1(\lambda)}{S_0(\lambda)}\right)^2 + \left(\frac{S_2(\lambda)}{S_0(\lambda)}\right)^2 + \left(\frac{S_3(\lambda)}{S_0(\lambda)}\right)^2}$. Therefore, PD(λ) = 1 would describe completely polarized light and PD(λ) = 0 would describe completely unpolarized light. Additionally, for the cases 0 < PD(λ) < 1, the unpolarized contribution (UP) is simply UP(λ) = 1 – PD(λ). Essentially, the technique requires only the addition of an achromatic quarter-plate and an achromatic polarizer just before the detector in a standard system for optical spectroscopy. The Stokes technique was applied to emitted fluorescence following continuous polarized 633 nm excitation. These measurements were split into three categories: measurements of P(NDI2OD-T2) prepared in solutions, spin-coated films (thicknesses of ≈ 80 nm) and drop-casted films (thicknesses of ≈ 2 μm). Each FL spectrum is obtained in a range of wavelengths (in our case, from 700 nm to 913 nm) and is fitted by the wavelength-dependent relation: $I(\lambda, \theta) = \frac{1}{2}\left[\left(S_0(\lambda) + \frac{S_1(\lambda)}{2}\right) + \frac{S_1(\lambda)}{2}\cos(4\theta) + \frac{S_2(\lambda)}{2}\sin(4\theta) - S_3(\lambda)\sin(2\theta)\right]$, where θ is the quarter-plates rotation angle. Therefore, we obtain a set of $\frac{S_i(\lambda)}{S_0(\lambda)}$ (for i = 1, 2 and 3) from which integrated areas (IA) and PD can be obtained in a range λ and λ + dλ. The ratio $IA\left(\frac{S_i(\lambda)}{S_0(\lambda)}\right)$ indicates the percentage of the detected FL that is polarized in: (1) vertical and horizontal directions $\left(\frac{S_1(\lambda)}{S_0(\lambda)}\right)$; (2) ±45° directions $\left(\frac{S_2(\lambda)}{S_0(\lambda)}\right)$; and (3) circular to the left and to the right $\left(\frac{S_3(\lambda)}{S_0(\lambda)}\right)$, see Table S1 in the supplementary information.

We have analyzed the $S_0(\lambda)$ and PD spectra for close to 200 FL spectra from several different samples and positions over the samples. The results are summarized in Figure 14, where once again the green stripes, blue stripes and red stripes delimit regions where ICs, Agg I and Agg II are expected, respectively. Figure 02(a) shows the $S_0(\lambda)$ parameter as a function of wavelength. The $S_0(\lambda)$ curves for the solutions (top row) present a behavior similar to those observed by Steyrleuthner and co-authors [37]: CN solutions are composed of primarily ICs, which emits around 720 nm, DCB solutions contain all the three species emitting around 720 nm (ICs), 780 nm (Agg I) and 825 nm (Agg II), and Toluene solutions which are expected to be composed of ICs and Agg II but the only peak appearing in the FL emission is referent

to Agg II, which emits around 825 nm. The $S_0(\lambda)$ data for the spin-coated films (middle row in Figure 14 (a)) clearly suggests the presence of three different peaks. The first peak, which appears around 720 nm is assigned to the IC, the second peak around 780 nm is assigned to Agg I, and the third peak at around 830 nm is assigned to Agg II. These results agree well with the absorption experiments for spin-coated films. Moreover, the increased intensity of Agg I and Agg II FL emissions support the hypothesis that in drop-cast films aggregate formation is favored. The set of results presented in Figure 14(a) lead us to very interesting conclusions: by comparing the top (solutions) and the middle (spin-coated films) plots for $S_0(\lambda)$, we have the first indication that efficient energy transfer mechanisms, such as exciton transfer or radiation re-absorption, is happening in solution. In fact, from the absorption data, one can immediately conclude that IC absorbs resonantly around 633 nm, Agg I absorbs resonantly around 710 nm, and Agg II absorbs resonantly around 815 nm. However, it is fundamental to recall that we do have a resonance window for each of these peaks, and the absorption data shows that there is an overlapping between the resonance windows for the IC and Agg I species, and an overlapping between the resonance windows for the Agg I and Agg II. Note that there is no overlapping between the resonance windows for IC and Agg II species. Therefore, by exciting at 633 nm, IC species are being resonantly excited and Agg I species are being excited in partial resonance. Agg II species cannot be excited by 633 nm radiation. Instead, any emissions carrying Agg II signatures can only be triggered by processes such as energy transfer, FL reabsorption and exciton transfer. Note that IC and Agg I species can also be excited via these processes but we believe that since they are being directly excited by the laser (even though Agg I is only in partial resonance), the FL reabsorption mechanism will be a minor effect. When we look at the spin-coated films we see all three peaks, which suggest that energy transfer is not as efficient in these systems (see Fig. 02(a) middle panel).

Additionally, by considering that ICs exist in spin-coated films casted from DCB and toluene solutions, we can conclude that such IC species were already stable in the solutions. In fact, since the solutions present larger optical paths when compared to spin-coated films, we believe that in solution the

energy transfer via radiation re-absorption [6, 11] is the most likely process taking place. These energy transfer mechanisms help us understand why the FL emissions from IC and Agg I species in Toluene-based solutions are quenched. Provided that the energy transfer mechanisms from IC and Agg I to Agg II are efficient, we have no reason to believe that there is full aggregation of IC into Agg I and then into Agg II as previously assumed in [37]. Therefore, we conclude that the spin-coated samples cast no doubt that all three species (IC, Agg I and Agg II) coexist regardless of the solvent used. It is also interesting to observe that the spin-coated films present a quasi-homogeneous $S_0(\lambda)$ emission for all the species (IC, Agg I and Agg II), again regardless of solvent choice. Because reabsorption processes are unlikely in spin-coated films (recall that spin-coated films present the smallest thickness), we attribute this result to the coexistence of the three different species (IC, Agg I and Agg II) with different concentrations and emission quantum yields. Next, looking at the bottom graphic in Figure 14(a), we see that the energy transfer process is also present in drop-cast films. Moreover, by recalling that drop-cast films are micron-thick, and that the solvents have fully evaporated, we deduce that the $S_0(\lambda)$ spectra also suggests that the aggregation process is intensified. This interpretation agrees with the results observed for the absorbance spectra (see Fig. 01).

The FL emission (and, therefore, the $S_0(\lambda)$ spectrum) is expected to be fully polarized, partially polarized or unpolarized, which must be described by the $PD(\lambda)$ [1, 10]. In order to analyze the $PD(\lambda)$ spectra, we discuss the results for solutions, spin-coated and drop-casted films, respectively. Figure 14(b) shows the $PD(\lambda)$ as a function of λ, acquired for the three different solvents. Our data shows that about 50% to 65% of the FL emitted from our samples has well-defined polarizations spanning from linear to circular, which are centered at distinct wavelengths, see Table S1 in the supplementary information. Note that $PD(\lambda)$ is an indirect measure of the organization of the sample's constituents. In order to make such analysis, one needs to compare the polarization of the incident light (in our case, vertical polarization) with the polarizations of the FL signal. On top of that, one needs to consider the following cases:

Case 1 (samples morphologically aligned – Full Alignment):

(1.1) for a sample in which the IC, Agg I and Agg II are aligned in a preferential direction, PD is expected to be 1 (or 100% polarized) provided the incident polarization is parallel to the direction of alignment. On the other hand, if the incident polarization is perpendicular to the direction of alignment, PD is expected to be zero. We must remember that we are analyzing the FL emission, which will only occur if the constituent absorbs the incident light. If no constituent absorbs light, there will be no FL emission. In the basis of this analysis, if the incident polarization is at 45o with the direction of alignment, the PD is expected to be 0.5 (or 50% polarized). If the incident light is polarized somewhere between 0 and 45o or 45o and 90o, PD should be between 1 (100 % polarized) and 0.5 (50 % polarized).

Case 2 (samples morphologically aligned – Partial Alignment):

(2.1) for a sample in which one of the species is aligned in a preferential direction and the remaining species are randomly aligned, the PD is expected to be 1 (or 100 % polarized) in the correspondent spectral region if the incident polarization is parallel to the direction of alignment of the aligned specie. For the spectral region referent to the other two randomly aligned species, PD is expected to be 0.5 (or 50% polarized). If the incident light polarization is perpendicular to the aligned specie, PD in the spectral region referent to the aligned species is 0 and again, for the spectral region referent to the other two species, PD is expected to be 0.5 (or 50 % polarized). If the incident light is polarized at 45o to the aligned specie, the PD should be 0.5 (or 50 % polarized) for all the species. Finally, if the incident light is polarized somewhere between 0 and 45o or 45o and 90o, the PD should be between 1 (100 % polarized) and 0.5 (50% polarized) for the aligned specie, and 0.5 (50% polarized) for the remaining species.

(2.2) for a sample in which two species are aligned in a preferential direction and the remaining specie is randomly aligned, PD is expected to be 1 (or 100 % polarized), in the correspondent spectral region, if the incident polarization is parallel to the direction of alignment of the two-aligned species.

For the spectral region referent to the other randomly oriented specie, PD is expected to be 0.5 (or 50 % polarized). If the incident light polarization is perpendicular to the two-aligned species, PD in the spectral region referent to the two aligned species is 0 and again, for the spectral region referent to the other species, PD is expected to be 0.5 (50 % polarized). If the incident polarized light is at 45o, PD should be 0.5 (50% polarized) for all the species. Finally, if the incident light is polarized somewhere between 0 and 45o or 45o and 90o, PD should be between 1 (100 % polarized) or 0.5 (50% polarized) for the two aligned species, and 0.5 (50% polarized) for the remaining specie.

Case 3 (fully misaligned samples):

(3.1) for a sample in which the IC, Agg I and Agg II are randomly oriented (in other words, no preferential direction of alignment for the species), PD is expected to be 0.5 (50% polarized) throughout the whole spectral region.

Case 4 (Solution samples):

(4.1) this case is identical to case 3 with the exception that in solutions the species can diffuse translationally and rotationally with diffusion rates that are dependent on the solvent's viscosities and constituent dimensions. Such diffusion may cause depolarization. Therefore, PD is expected to be between 0 (fully unpolarized) and 0.5 (50% polarized) throughout the whole spectral region.

As shown in Figure 14(b), which brings the PD associated to the FL signal as a function of wavelength, the state of polarized light in the FL emission spans over a broad spectral range and more importantly: it is possible to control the light's PD(λ) by manipulating the samples according to solvent and/or if the samples are in solution or thin/thick films. Per definition, PD(λ) is independent of the densities of species present in each case (in other words, the quantity of each species emitting polarized light). Therefore, the information we obtain from PD(λ) is purely related to morphological structuration, energy and charge transfer mechanisms, and to depolarization caused by diffusion. As seen in Figure 14(b) top panel, toluene solutions emit polarized light mostly in the spectral range referent to Agg II

species, while DCB and CN solutions emit polarized light throughout the whole spectrum which comprises emissions in the range of the IC, Agg I and Agg II species. It is important to comment that solutions are expected to contain randomly oriented species that diffuse translationally and rotationally with time *(without diffusion, a PD(λ) of 0.5 would be expected)*. However, it is also important to pay attention to two factors: the viscosity of the solvents and the densities of the constituent species. In our case, the viscosities of the solvents we used follow, from the highest to the lowest viscosity, Toluene<DCB<CN. This means that a particular species, say IC, will less readily diffuse in CN when compared to Toluene. On the other hand, if we fix a particular solvent, ICs are expected to diffuse more easily than Agg I and Agg II, since the aggregates are denser than the ICs. Solutions will follow case 4 described above. As seen in Fig. 02(b) top panel, PD(λ) in the IC region (green stripe) is about 0.55 in the CN-solution, is 0.5 to 0.25 with decreasing λ in DCB and is about 0.13 in toluene. These results for IC are within our claims above: ICs will be random in all the solutions but in CN they will present lower diffusion when compared to ICs in DCB and toluene, and the ICs in DCB will present lower diffusion when compared to toluene. Therefore, in toluene we may expect high depolarization when compared to DCB and CN, having DCB presenting an intermediate depolarization compared to the other two.

Not surprisingly, Agg I species will diffuse with more difficulty and depolarization effects are expected to be lower. In the Agg I region (blue stripe) the PD(λ) curve for the DCB solution essentially reaches the same values observed for the PD(λ) from CN solution and then goes a little bit over reaching 0.6, indicating a decrease in the randomness of the species, which is consistent to a loss of efficiency in diffusive behaviors. It is important to recall that although the PD(λ) for the CN solution matches the PD(λ) from the DCB solution, the species emitting in CN in this Agg I region are still ICs with different chain sizes (CN solutions primarily have ICs). Therefore it is reasonable to conclude that PD(λ) for the CN solution keeps the same behavior reported earlier for the region where all the solutions possess ICs. Following the same reasoning, it is not surprising that the PD(λ) for the Toluene solution increases for the same reason PD(λ) increased for the DCB solution. It is also not surprising that such an increase is less

effective in the Toluene solution since Toluene has the smallest viscosity among the solvents. In the Agg II region (red stripes), PD(λ) for both DCB and Toluene solutions reach 0.6 and then starts decreasing as λ increases from 850 nm.

It is important to discuss why PD(λ) decreases for wavelengths above 850 nm. The FL emissions in this region come from long IC, Agg I and Agg II species and it is known from the literature that long-sized polymeric structures, regardless if they are ICs or aggregates (which are formed by ICs) present a broad distribution of conjugation lengths [78-80]. The oligomers referent to these conjugation lengths are connected via defective sites and intra-chain exciton transfer from one conjugated unit to another. We excite our samples at 633 nm, which correspond to resonances with small IC´s conjugated units. Therefore, long conjugated units can only be excited via either exciton-transfer or re-absorption processes, and such processes are known to cause a wavelength-dependent depolarization rate ($\partial PD(\lambda)/\partial\lambda$), which is essentially the same for all the curves, since it is caused by the mechanism discussed above [6, 11, 81]. Next, we explain why the CN based solutions PD(λ) appears below the DCB and Toluene PD(λ) curves at larger wavelengths. As explained above, in order to find PD(λ) we have to consider the ratio between $S_1(\lambda)$, $S_2(\lambda)$ and $S_3(\lambda)$ with $S_0(\lambda)$. It happens that the FL emission tail for the CN-solution, which contains only ICs, approaches zero very quickly above 850 nm since ICs are no longer efficiently emitting in that region. Therefore, we have a considerable increase in the indeterminacy of the ratios $S_i(\lambda)/S_0(\lambda)$ for i = 1, 2 and 3.

Figure 02(b) middle panel shows the PD(λ) results for the spin-coated thin films. Regardless of solvent used, all the curves follow similar behaviors in all the three regions: IC, Agg I and Agg II regions. The obtained PD(λ) results are in agreement with the morphological structuration of thin films as discussed by Takacs *et al.* [82, 83]. In their manuscripts, they show that thin films are organized in domains (lamellae), and domains formed by ICs are amorphous (with no preferential orientation for the ICs in a particular domain), while domains formed by aggregated species keep a preferential orientation within a particular domain. Each spin-coated film will contain several distinct domains that are, among

themselves, randomly oriented despite their individual, well-organized structures. Since we are probing our samples in the micron-scale, we are measuring an average of several different domains randomly oriented, which brings us to case 3 described above. We see in Figure 14(b) middle panel that for all the spectral regions PD(λ) is between 0.4 and 0.5. The difference observed in the PD(λ) values for spin-coated films, when the spectra goes from 700 nm to 850 nm, is assigned to polarized emission due to different domains with amorphous domains formed by ICs species (around 700 nm) emitting less polarized light than the FL emitted from organized domains (region around 800 nm). It is also important to comment that, the same decreasing rate in PD(λ) with increasing wavelength, for wavelengths beyond 850 nm, is observed. This indicates that the depolarization mechanisms around that spectral range are in fact coming from exciton and energy transfer phenomena among species with different sizes and conjugation lengths.

Finally, Figure 14(c) bottom panel brings PD(λ) for drop-cast thick films. Differently from spin-coated films, drop-cast films can only be solvent-free after the solvents evaporate. Such evaporation happens more easily for Toluene than for CN, for example. As the solvents evaporate, the species have more time to aggregate and we clearly see from $S_0(\lambda)$ that in CN the ICs are being converted into Agg I and that in DCB the ICs and Agg I species are being converted to Agg II. These conversions from IC to Agg I in CN and from Agg I to Agg II in DCB are expected since Agg I species, as discussed above, are an intermediate case between IC and Agg II. Additionally, such thick films obtained via drop-cast have more efficient energy transfer mechanisms (re-absorption). This explains why in the $S_0(\lambda)$ spectra we have a small emission in the IC region for films made from the CN solution, and a negligible emission for films made from DCB and Toluene solutions. This also explains the enhancement in the relative emission from the Agg I region in CN films and the decrease of the relative emission from Agg I in DCB films. Regarding PD(λ), it is paramount to remember that drop-cast films follow the case 3 described above, with analogous explanations as for the spin-coated samples. Therefore, the differences observed for PD(λ) in the IC region (green stripe) around 700 nm, for CN, DCB and toluene films can be understood

by considering the very low intensity of the FL emission from DCB and Toluene films in this region. This low intensity is expected since we have aggregation of ICs in drop-cast films for these solvents as discussed above and this low intensity also causes indeterminacy in PD(λ).

d. Paper 1: Conclusion

Summarizing, we have employed a new experimental approach called Stokes Spectroscopy that allowed us to measure the polarized fluorescence emission of P(NDI2OD-T2) within the scope of Stokes theory. Details of the state of polarized light in the fluorescence emitted by the polymer were revealed by analyzing a broad range polarization degree spectra assigned to the polymer ICs and aggregates emissions. By changing the solvent type and by utilizing either solutions or thick/thin films, it is possible to control the polarization degree as a function of the wavelength for the emissions from the ICs and aggregates. The polarization degree has potential to be used as a quality assessment tool that allows for probing the microscopic structure of polymer films. It also has potential to probe depolarization effects caused by energy and charge transfer mechanisms. ICs and aggregates emit differently according to the conditions the polymer is exposed to. Such polarization-selective emissions due to distinct species indicates P(NDI2OD-T2) polymers are excellent candidates for coating optical elements such as lenses in sunglasses or glass windows, and can be used to provide different polarization degrees for emitted light, which is a useful feature for applications in screens and organic devices.

e. Paper 1: Figures

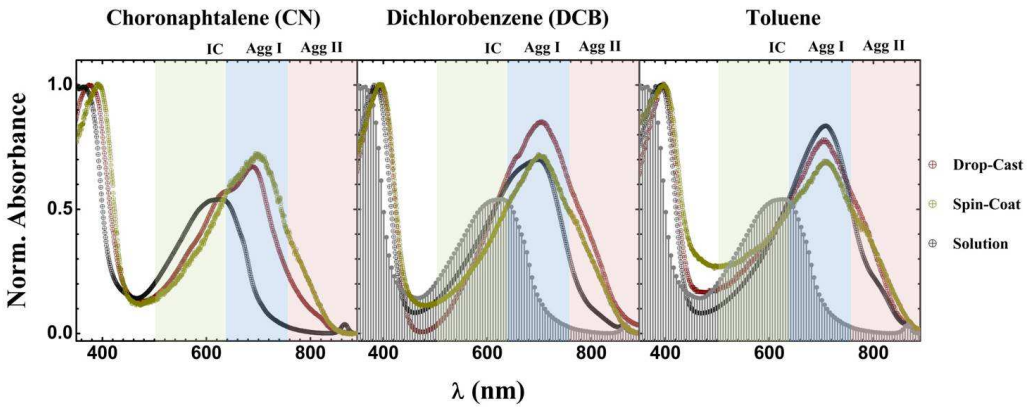

Figure 13. P(NDI2OD-T2) Absorbance Comparison

Absorbance of P(NDI2OD-T2) prepared in different solvents (Chloronapthalene, Dichlorobenzene, and Toluene). This figure allows us to compare the effects of sample thickness on a given solution, holding solvent choice steady. Here we begin to see the idea that the interaction with the surface has a meaningful effect on aggregate formation depending on solvent choice. Suggested regions for IC (green stripes), Agg I (blue stripes) and Agg II (red stripes) are added to help guide discussion [37]. The gray shaded graphs represent the spectrum acquired for CN solution and are plotted for comparison purposes. All the spectra are normalized by the π-π* transition band located around 400 nm.

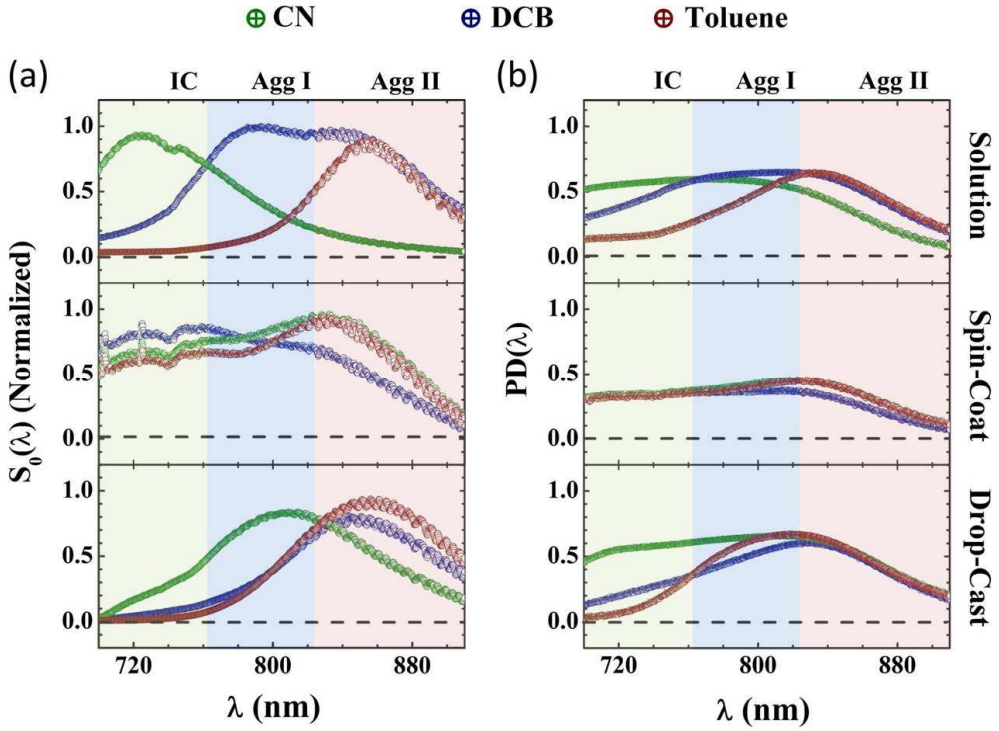

Figure 14. S0 and PD for NDI solution, spin coated and drop cast samples

The S_0 Stokes component and Polarization Degree (PD(λ)). Here we see the S_0 (left column) and Polarization Degree (right column) of P(NDI2OD-T2) prepared in different solvents (Chloronapthalene, Dichlorobenzene, and Toluene), comparing measurements in solution (top graphs), spin coated samples (middle graphs) and drop cast samples (bottom graphs). Recall, S_0 represents the measured intensity, while the PD(λ) is the amount of polarized emission (linear and circular) at a given wavelength. With this

in mind, the top most graph in the first column clearly shows the progression from IC species in CN based solutions to Agg I and Agg II in DCB, and finally predominately Agg II in toluene based solutions. Spin coating this solution (middle graphs), the S_0 measurements show the existence of all formations (IC, Agg I and Agg II) for all prepared solutions. Looking to the right column, we see evidence for the ability to tune polarized emission based upon solvent choice and film thickness. From here we begin to see evidence of the existence of all formations (IC, Agg I and Agg II) despite solvent choice as the polarization spans a broad wavelength range. Suggested regions for IC (green stripes), Agg I (blue stripes) and Agg II (red stripes) are added to help guide discussion.

f. Paper 1: Supplemental Information

Figure 15. Paper 1 Supporting Information FL Data top, middle and bottom plots the fluorescence (FL) intensity as measured. Note that, as discussed above and in the main text, the FL intensity and the Stokes S_0 parameters are proportional to each other [10, 51, 84].

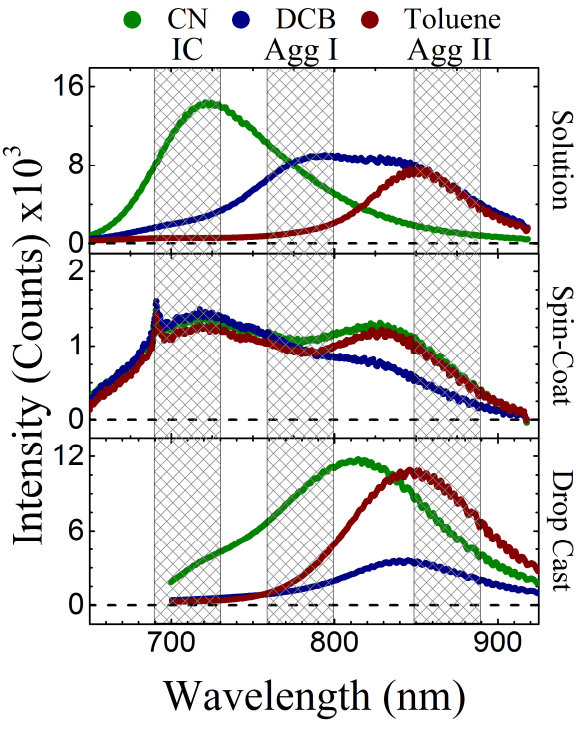

Figure 15. Paper 1 Supporting Information FL Data

Here we see the FL intensity of P(NDI2OD-T2) prepared in different solvents (Chloronapthalene-CN, Dichlorobenzene-DCB, and Toluene), comparing measurements in solution (top graphs), spin coat samples (middle graphs) and drop cast samples (bottom graphs).

Integrated areas of S_i/S_0 for i = 1, 2 and 3 in the IC (green stripe in Figure 14(b)), Agg I (blue stripe in Figure 14(b)) and Agg II (red stripe in Figure 14(b)) regions. Note that i=1 stands for horizontal /

Integrated areas (IA)	$\frac{S_1(\lambda)}{S_0(\lambda)}$	$\frac{S_2(\lambda)}{S_0(\lambda)}$	$\frac{S_3(\lambda)}{S_0(\lambda)}$	$\frac{S_1(\lambda)}{S_0(\lambda)}$	$\frac{S_2(\lambda)}{S_0(\lambda)}$	$\frac{S_3(\lambda)}{S_0(\lambda)}$	$\frac{S_1(\lambda)}{S_0(\lambda)}$	$\frac{S_2(\lambda)}{S_0(\lambda)}$	$\frac{S_3(\lambda)}{S_0(\lambda)}$
Solvents → / Species ↓	IC	IC	IC	Agg I	Agg I	Agg I	Agg II	Agg II	Agg II
Solution									
CN	48.3	3.1	3.7	23.2	5.3	1.3	30.9	4.9	1.3
DCB	20.1	1.3	2.6	23.1	4.2	1.3	43.3	5.2	3.2
Toluene	5.1	0.4	0.7	5.1	1.1	0.0	51.2	5.1	4.5
Spin coated									
CN	14.9	1.9	0.0	9.5	2.3	0.0	26.9	1.4	0.0
DCB	14.5	1.6	0.0	11.5	2.4	0.0	20.1	1.6	1.2
Toluene	14.9	1.2	0.0	8.8	3.3	0.6	26.7	3.6	0.9
Drop cast									
CN	17.1	0.3	0.9	28.3	3.8	1.5	50.6	2.8	0.7
DCB	0.0	0.0	0.0	10.6	4.6	0.9	49.7	12.8	1.8
Toluene	0.0	0.0	0.0	12.8	13.7	0.0	49.3	24.7	2.7

Table 1. Paper 1 Supporting Information Integrated Area Table

vertical polarizations, i=2 stands for ±45º and i=3 stands for circular to the left/right polarizations. With such values one can determine PD(λ) as described in the main text.

PAPER 2: PROBING H-, J-, AND HJ-AGGREGATE SPECTRAL SIGNATURES VIA STOKES FORMALISM FOR POLARIZED LIGHT: APPLICATIONS TO P3HT

a. Paper 2: Abstract

Spectroscopic measurements, particularly absorption and fluorescence (FL), have seen significant success in the characterization of polymer systems including poly(3-hexylthiophene) (P3HT). In particular, they have seen significant use as a means of probing H- and J- aggregate behavior in P3HT among other polymer systems. While excitonic transitions associated with these aggregate formations are readily obtained and visualized at low temperature (T<70K), thermal affects broaden their spectral signatures, making it difficult to accurately resolve signatures of one transition to another. Modeling, including Frank Condon fitting and numerical calculations by other groups have been able to deconvolute peaks from PL signatures, even from high temperature data (T>150K). However, these fitting techniques involve in depth fitting algorithms and do not necessarily interact directly with acquired PL signatures, instead providing best fit approximations. Here, we show how the Stokes Formalism can be applied to acquire polarization dependent spectroscopic emission, and that the off axis linear polarization (45-degree polarized light) shows heightened resolution of aggregate emissions typically unresolvable at high temperatures (T>150K). Subsequent analysis of this polarized emission is then used following proposed theory to obtain emission peak ratios, which have implications on coherence lengths, coherence numbers and inter / intra-chain binding parameters.

b. Paper 2: Introduction

The understanding and subsequent characterization of polymeric semiconducting devices has been of heightened interest as the drive for cost effective, high yield and easily process-able devices pushes research interests forward [6, 8, 9, 18, 85-89]. Emerging as a champion among such polymeric semiconductors is Poly(3-hexothiophene) (P3HT), a Regio regular, π-conjugated polymer system

[9, 21, 22, 25, 28, 41, 52, 53, 66, 85, 90]. Of particular interest in P3HT is its tendency to form semi-crystalline domains when cast as thin films, also known as aggregates, which are a product of π-π stacked chains. These aggregates are traditionally understood as intra- vs inter- chain phenomena, and are classified as H- and J- aggregates respectively. An interplay between H- and J- aggregate formation can also be realized through variation of the polymers inter and intra chain coulombic coupling (J_0), and is classified as an HJ- aggregate. [9, 19, 21, 22, 26, 27, 30-32, 52, 53, 66, 89-94]. The understanding of these types of aggregate formations is key in understanding the relationship between morphology, photo physics and charge carrier characteristics in P3HT and other polymer systems.

J-aggregates are understood as polymer formations in which neighboring chromophores (and therefore chains) are oriented in a tip to tail orientation of neighboring chains (see schematic representation in Figure 14A). Alternatively, in H-aggregates, chromophores are oriented in more of a stack, or side by side organization of neighboring chains (again, see Figure 14A) [9, 19, 21, 22, 25-27, 30-32, 52, 53, 66, 89-95]. Models suggesting an interplay of both aggregate types, or HJ- aggregates has also been suggested and theoretically demonstrated (Figure 14A) [27, 30, 32, 94]. Each type of aggregate formation is strongly related to the vibrionic coupling between the $S_0 \rightarrow S_1$ optical transition and the $\omega_o \sim 1{,}400\ cm^{-1}$ $(0.14eV)$ vinyl/ring stretching mode found in most π-conjugated organic polymer systems. However, the variations in excitonic coupling in the development of each aggregate formation results in varying spectral signatures. For example, the formation of J-aggregates is a result of negative excitonic (or Coulombic) coupling with $J_0 < 0$ (or $J_{intra} < 0$), which subsequently allows for 0-0 emission at low temperatures (the expression of which is affected by temperature). Alternatively, H-aggregate formations are a result of positive excitonic (or Coulombic) coupling with $J_0 > 0$ (or $J_{inter} > 0$), which leads to a strictly forbidden 0-0 emission at low temperatures (this transition can however be thermally activated). HJ-aggregates, while containing both formations, are also restricted in their expression of the 0-0 peak emission in the same way as H-aggregates [9, 24-32, 94]. It is important to note that HJ- aggregates demand a sort of co-existence of H- and J- aggregates, that is connected isolated

chains (J-aggregates) be stacked along the polymer plain (H-aggregation) (see Figure 14A). A more detailed description is provided by H. Yamagata and F. C. Spano, which suggests that J-, H-, and HJ-aggregates signature are altered with variation of the J_{inter} and J_{intra} parameter in their theoretical modeling. This will be particularly important and expanded upon below.

Development in the theory surrounding H-, J-, and HJ- aggregate behavior has made it possible to obtain information about prepared films. For example, it has been shown that the ratio of the emission peak intensity of the 0-0 and 0-1 transitions ($I_{PL}^{0-0}/I_{PL}^{0-1}$) can be used to determine the Coherence number (N_{coh}) and/or coherence length (l_0) in prepared P3HT films and solutions, both of which are intimately connected to disorder (and therefore charge transport in applications). In H- (J- and HJ-) aggregates, it is understood that these emission peak positions blue shift (red shift) with increasing temperature, and their ratio increases (decreases) with the same increase in temperature. Emissive peak positions and ratios are readily available at low temperature (T<75K), as peaks can be easily resolved from one another. However, as temperature increases, spectral broadening of these emission peaks makes direct analysis essentially impossible. Instead, sophisticated fitting techniques, including Frank Condon modeling and numerical analysis, are frequently implemented to obtain such information [6, 13, 24-32, 66, 86, 91, 94, 96]. The goal of this work is to show how such information (H-, J- and HJ- Aggregate signatures) can be recognized through the acquisition and subsequent analysis of polarized emission as described by the Stokes formalism of polarized light. Via this technique we also show that films of P3HT, beyond presenting H-aggregates signature, contain signatures of HJ-aggregates, which to the best of the authors' knowledge is being observed for the first time in this type of polymer.

Measurements of polarization dependence can traditionally involve variation of an incident sources polarization or sample rotation, or instead the placement of a polarizer following excitation and radiation to serve as an analyzer [6, 9]. However, these methods are only probing intensity variations, and while they can be used to get some sense of a polarization state related to a particular polarization (for example, circular or ±45° polarization), they are limited in their scope. The Stokes formalism, is able to deliver the polarization landscape of a spectroscopic signature in a way which provides further insight

when compared to traditional methods since it considers simultaneous analysis of each type of polarization: linear horizontal and vertical; linear ±45°; and circular to the left and right. In other words, this method breaks light into four distinct parameters, giving information about intensity (S_0), vertical or horizontal polarization (S_1), ±45° polarization (S_2), and left or right circular polarization (S_3). The method is particularly useful in that these parameters can be directly related to measurements of a sources emission intensity. Following the formalism, and putting to use common optical components (in this studies case, a rotatable quarter wave plate and a horizontally aligned linear polarizer), one can directly acquire the previously described polarization parameters from a series of measurements of a sources emission [2, 5]. In this manuscript, we will show how the use of this formalism, and particularly the expression of S_2 ($\pm 45^o$ emission), can provide heightened resolution of aggregate emission peaks, even at elevated temperatures (T≈300K). This method is novel, in that obtained peaks are acquired through direct non-invasive and non-destructive measurements of emission spectra, circumventing the need for numerical analysis, quantum mechanical fitting methods and expensive low-temperature measurement apparatus.

c. Paper 2: Results and Discussion

Samples were prepared by adding 1mg of P3HT (Sigma Aldrich MW) in 1mL of Chloroform stabilized with amylene (Fisher Scientific, > 99.8%). Samples of approximately 0.1mL were then prepared on ~1cm^2 glass slides to create drop cast samples. An additional set, following the same scheme were spin coat at 2000rpm for one minute. All samples were then subject to vertically polarized 532nm, steady state excitation at various locations and sample rotations. The PL emission was captured and subject to Stokes analysis (see SI for more information) allowing for intensity and polarization state analysis.

Figure 14B shows a representative fluorescence (FL) intensity spectra of a drop cast P3HT film measured at room temperature (T≈300K) as acquired (PL) and after processing through the Stokes formalism (S_0), normalized to the maximum of each respective peak. Recall that S_0 within this framework

is equivalent to the total intensity. The intensity discrepancy can be attributed to smoothing effects from application of the stokes formalism and the defined wavelength dependence of the achromatic quarter wave plate and linear polarizer setup (while they are "achromatic" within the required spectral range, there is still a wavelength dependence, with varying transmission coefficients). This PL signature has been demonstrated thoroughly for P3HT by various studies, the approximate positions of the 0-0, 0-1, and 0-2 excitonic transitions for H-aggregates (when measured at low temperatures) have been labeled following their assignments [26-31]. This is the crux of the problem for traditional measurement methods: elevated temperature broadens these signatures, making the emission peaks broaden and overlap each other's range. Visualizing or fitting gaussians to such peaks, while possible, requires numerical calculation and/or Frank Condon fitting for heightened accuracy. These fitting procedures therefore require previous assignment of H-, J- or HJ- aggregation to guide calculations. We show later that presuming of one type of aggregate or another within those fitting techniques is incomplete, and further consideration must be taken.

We now turn our attention to Figure 15A, which has the same S_0 spectrum (the Stokes formalism representation of intensity) from Figure 14B with the addition of the normalized S_2 spectrum (normalized to the S_2 parameters highest peak). Notice that the peak positions of S_2 match nearly perfectly, the previously labeled transitions (0-0, 0-1, and 0-2) form H-aggregate models. They are in fact blue shifted slightly from positions in literature, which is expected with increased temperature for H-Aggregates in P3HT [26-31]. In this case, we chose to take the modulus of S_2 for ease of viewing; however, for H-Aggregates peaks we see negative values in S_2. Also of note is the relative heights of the peaks, namely the ratio of the 0-0 to 0-1 peaks. It has been shown for H-aggregated P3HT that the ratio of the 0-0 to the 0-1 emission peak is zero at low temperature (T<5K), and increases with temperature reaching unity at maximum. Fitting gaussians to these peaks (an example of this is shown in Figure 15B), and extracting the peak height(s), we can obtain a ratio of approximately 0.4, this ratio agrees well with the expected 0.3 to 0.6 range (more detailed peak information is provided in Table 2) [26-32]. Through a series of measurements (over 50 measurements, including different sample positions and rotations), we acquire

ratios ranging from 0.1 to 0.5, averaging close to 0.3. Variations can be attributed to local ordering / conditions (expanded upon further below). From here, one can follow the prescription suggested through a series of studies by Spano et al. [24-32, 91, 94] and fit this ratio to the following:

$$\frac{I_{0-0}}{I_{0-1}} = (\sigma W)^2 \frac{1-\beta}{1+\beta} \frac{\left(1 - \frac{0.24W}{\hbar\omega_0}\right)^2}{\left(1 - \frac{0.39W}{\hbar\omega_0}\right)^2} \quad (1)$$

Here, β is related to the correlation length (l_o), $l_o = \frac{1}{\ln(\beta)}$. σ is related to the line width of fit peaks, ω_o is $\sim 1{,}400\ cm^{-1}$ $(0.14eV)$ (associated with the vinyl/ring stretching mode found in most π-conjugated organic polymer systems), and W is related to the interaction energy J_o of the aggregate. Equation (1) was developed to relate the peak intensity ratio for ***H-aggregates*** to conditions within the film. Following this prescription, we can acquire the correlation length, which is useful within device fabrication. For the example measurement above (in Figures 15), and assigning theoretical values for W and ω_0 from other studies, we obtain a correlation length of ~5.3nm, which agrees extremely well with literature [26-32].

Let us now turn to Figure 16A, which shows another acquisition of the S_2 stokes parameter for the same P3HT sample as considered previously, measured at the same position. However, ***for this measurement, the sample was rotated by 90 degrees, and all other measurement conditions were maintained***. The representation of the S_2 parameter is again normalized but this time the modulus is not taken. It is important to note that in this case the S_2 spectra is dominated by two positive peaks which are offset with relation to the three peak positions observed in Figure 15. A closer look at Figure 16A reveals two dominant peaks between the 0-0 and 0-1 peaks, and the 0-1 and 0-2 peaks assigned to H-aggregates (see Figure 15B). Another striking difference is the relative heights of the two peaks are approximately the same. Following the same gaussian fitting procedures as before, we acquire the centers of these peaks, and find that they match well with the 0-0 and 0-1 peaks assigned, *a priori*, to J-type aggregates in P3HT [27, 30-32, 41, 66]. Provided these peaks were due to the existence of purely J-aggregates, one could

follow the prescription presented by Spano et. al. and fit these peaks to the following ratio, which compares the intensity ratio of the 0-0 to 0-1 peaks:

$$\frac{I_{0-0}}{I_{0-1}} = \frac{N_{coh}}{S} \qquad 2$$

Here, N_{coh} is the exciton coherence number, and λ_o^2 is the Huang-Rhys (HR) parameter for the polymer in question (for P3HT, this number is set to 1) [9, 27, 30-32, 41, 66]. ***This expression is for J-aggregates only***, and following its application to the spectroscopic signature in Figure 16A, we obtain $N_{coh} \approx 0.95$. This value is lower than expected for isolated chains or J-aggregates, as expected values are greater than one for low temperatures and approach unity at increased temperature (~300K). This discrepancy can however be resolved through the HJ- aggregate model proposed by H. Yamagata and F.C. Spano [32]. Essentially: The H-like behavior from before (Figure 15) remains in the film and requires the existance of J_{inter}, or put differently ***the polymer chains (or J-aggregates) are in fact lined in a stacked formation and are therefore better described as HJ-aggregates***, not isolated chains. The requirement for this J_{inter} therefore alters the expression from that of isolated chains (J-aggregates) to stacked chains (HJ-aggregates), in doing so, the ratio of $\frac{I_{0-0}}{I_{0-1}}$ is permitted to fall below one. The presence of J_{inter} also affects the expression of H-aggregates as well, and is what allows for the ratio of the H-aggregate peaks to be less than 1 at high temperatures (~300K) (as seen in Figure 15). The scaling of the ratios of the 0-0 to the 0-1 PL for HJ- aggregate peaks follows:

$$\left(\frac{I_{0-0}}{I_{0-1}}\right)_{max} = \frac{1.35}{\lambda_0^2}\sqrt{\frac{|J_{intra}|}{J_{inter}}}. \qquad (3)$$

The 1.35 comes through fitting parameters detailed by H. Yamagata and F.C. Spano and λ_0^2 is again the HR parameter [32]. H This relation, when considering the simultaneous existence of H- and J-aggregates in prepared films (or HJ-aggregates) is what permits the existence of a ratio less than 1 for peaks traditionally assigned to J-aggregates. Put another way, we are showing that in prepared films, there are no isolated chains, but instead HJ- aggregates, and the ratio of J_{intra} and J_{inter} dictates the ratio of the

0-0 and 0-1 PL intensity peaks. The literature states that drop cast films should favor H-type aggregates, but none the less we clearly find evidence for HJ-like aggregates behavior [9, 22, 27, 28, 30, 32]. It is important to comment why we see three slightly negative peaks in Figure 15A. Essentially: The H-like behavior from before isn't completely absent, however, it is much less prominent in this case (due to excitation conditions / local order), so it may still appear despite this orientation favoring emission from the HJ- transition peaks.

To further illustrate the coexistence of H-aggregate and HJ-aggregate emission peaks, we go to Figure 16B. This is again the same sample and position as the previous measurements, however the sample is rotated by 50 degrees with relation to the original angular position (0 degrees) that led to the results presented in Figure 15. The signal was again normalized, however by the absolute value of the lowest peak (which was negative in S_2). This results in the lowest peak presenting a negative height of -1. Because the positive expressions of S_2 didn't reach the same height, we see positive values reaching slightly over 0.5 instead of 1. Note that this doesn't affect analysis, and is done only to make figures easier to interpret. The peculiar thing for this position is: we can clearly identify features from H- and HJ-aggregates, the H-aggregate peaks presenting as negative S_2 values, and HJ-aggregate peaks as positive values. Again, we determine that the positive peaks are not J-aggregates as the ratio of the intensity's of the 0-0 to 0-1 peaks is less than one, indicating the existence of J_{inter} which necessitates the distinction between isolated J-aggregates and stacked chains (HJ-aggregates). The positive and negative values for the HJ- and H- aggregate peaks within the S_2 spectra is explained through the 90 degree offset between H- and J- chains in the HJ- model from Figure 14. The ratios of the 0-0 to 0-1 peaks for each case (H- or HJ-aggregates) once again agrees with expected values: 0.33 and 0.91 for H- and HJ-aggregates respectively (see Table 1 for more detailed information). This brings us to the following conclusion: local orientation and organization will dictate the expression of aggregate formation for off axis emission. Put another way: H-aggregate signatures (as in Figure 15A); HJ-aggregate signatures (as in Figure 16A), and simultaneous H- and HJ-aggregate behavior (as in Figure 16B) are all possible in drop cast films of P3HT given correct excitation conditions. This however doesn't mean that both formations are in equal

proportion to one another. For example, in the presented film data, probing around its surface at various locations and rotations shows predominantly HJ- aggregate behavior in S_2. With different rotations and positions, it is possible to find exclusively HJ-aggregate behavior (as in Figure 16A), simultaneous H- and HJ- aggregate expression (such as Figure 16B), or exclusively H-aggregate behavior as in Figure 16, however most positions and rotations yield exclusively HJ-aggregate signatures. Specifically; ~25% of measurements presented exclusively H-aggregate signatures (such as Figure 15), ~40% exclusively HJ- (such as Figure 16A) and ~35% simultaneous expression of H and HJ-aggregates (such as Figure 16B). Assuming that the film is predominantly of the HJ-aggregate type might be a good approximation; however, local environment and conditions will affect this. To provide more clarity on these local variables, Figure 17 shows a series of measurements on the same sample through rotation of 90 degrees (in 10 degree increments). Diving S_2 by S_0 and the modulus of each graph helps to provide clarity, allowing that the individual peaks can be recognized for H and HJ like behavior as described above.

Spin coated samples are primarily important for fabricating organic devices such as solar cells or organic light emission devices (OLED) [21, 25-30, 94, 96]. It is known that P3HT self-assembles during the drying process to generate solid films. The realization of how polymers aggregate in films is, therefore, fundamental. Spin coated films are expected to present both H- and J-aggregates with H-aggregates being the dominant species [21, 25-30, 94, 96]. To test this, we can look to spin coated samples, from the point of view of the Stokes method [25-30, 32, 52, 96]. Figure 18 shows S_2 measurements from such a film, at the same position and different rotations. We can clearly see, the expression of HJ-aggregate behavior (0 degree sample rotation), to both H- and HJ- behavior (40 degree rotation), to predominantly H-aggregate behavior (90 degree sample rotation). H-aggregation was predominantly seen as sample rotation changed from 0 to 90 degrees, with simultaneous expression of H- and HJ- aggregates as transition from HJ- to H- occurres (from 30 to 50 degrees). Probing around the sample, we found more emissions suggesting H-aggregate behavior, however there are areas where exclusively HJ- aggregates and simultaneous H- and HJ-aggregate behavior exists. Approximately 50% of measurements were H-type, 30% showed simultaneous H- and HJ-aggregate expression and 20% were

	Transition	0-0 (H)	0-1 (H)	Ratio 0-0/0-1	0-0 (J)	0-1 (J)	Ratio 0-0/0-1
0 Degree Rotation	Peak Hight	0.32±0.1	0.82±0.2	0.39			
	Width	10.6±0.5nm	13.4±0.4nm				
	Center	654.3±0.5nm	712.8±0.2nm				
50 Degree Rotation	Peak Hight	-0.27±0.2	-0.82±0.2	0.33	0.59±	0.65±0.2	0.91
	Width	27.0±	9.6±1nm			12.2±0.5nm	
	Center	651.9±0.4nm	712.6±0.3nm		680.2±0.3nm	744.5±0.3nm	
90 Degree Rotation	Peak Hight				0.84±0.04	0.88±0.02	0.95
	Width				14.6±0.8nm	13.6±0.3nm	
	Center				680.8±0.2nm	743.4±0.2nm	

Table 2. Select Drop Cast Sample Peak Information

exclusively HJ-aggregates. This further solidifies the claim that local environment and excitation conditions are of heightened importance as different aggregate formations can be accessed. Note that once again the $I_{0\text{-}0}/I_{0\text{-}1}$ ratio for both H- and HJ-aggregates agrees very well with the values reported in the literature, with $N_{coh} \approx 0.43$ for H-aggregates, and a ratio of ~0.75 for HJ-aggregates. Table 2 summarizes this information.

The remaining question is: why does acquisition of 45-degree emission (the S_2 Stokes parameter) provide heightened resolution of these exitonic transition signatures? Traditionally, one expects polymer chains and chain aggregates which are oriented with their backbone / axis aligned with an exciting sources polarization, to be more readily excited [6, 21, 26-31, 41]. Subsequent emission from species associated with those same chains / aggregates is then expected to be polarized along the same polarization direction [6]. Following this line of thinking and applying it to measurements of P3HT, one would expect the majority of measured emission to be from that of vertically aligned aggregates / chains. Within the Stokes formalism, this would be realized as negative values of the S_1 parameter. Figure 19 shows the modulus of S_1, normalized to its peak value, plotted along with the overall emission S_0. The

	Transition	0-0 (H)	0-1 (H)	Ratio 0-0/0-1	0-0 (J)	0-1 (J)	Ratio 0-0/0-1
0 Degree Rotation	Peak Hight				0.58±0.06	0.77±0.06	0.75
	Width				21.6±2nm	17.0±0.4nm	
	Center				688.0±0.3nm	738.7±0.2nm	
40 Degree Rotation	Peak Hight	0.088	0.14	0.63	0.72	0.74	0.97
	Width	7.16	97.55		21.65	30.94	
	Center	651.9±0.4nm	712.6±0.3nm		680.2±0.3nm	744.5±0.3nm	
90 Degree Rotation	Peak Hight	0.37±0.09	0.86±0.03	0.43			
	Width	30.7±	15.5±0.8nm				
	Center	659.0±0.5nm	713.8±0.3nm				

Table 3. Select Spin Coat Samples Peak Information

modulus is taken for clarity, but for all measurements, the S_1 parameter is negative, expected for vertical emission and chains / aggregates aligned with the exciting source. S_1's shape nearly matches that of S_0, which is also expected as it is the majority of the emission from our sample (the inset shows that this emission accounts for approximately 50% of the overall emission). Another reason for lowered vertical emission is that these excited chains (and aggregates) can subsequently transfer energy via non-radiative processes to off axis chains and aggregates (off axis compared to the excitation source) [9]. The end result is that we can reliably say that mostly those chains / aggregates aligned with exciting sources polarization are excited and subsequently emit. However, as shown in the inset of Figure 19, S_1 doesn't perfectly match S_0, because there are other polarization directions contributing to the emission as well as unpolarized emission. As shown previously in Figures 15, 16, 17 and, there is off axis emission, in this case ±45º emission represented by the S_2 Stokes parameter. Direct excitation of these off-axis chains / aggregates is possible, if one takes the projection of the incident polarizing source onto the chain length (this would follow a cosine squared dependence). Another possibility would be energy transfer between neighboring chains, which has been documented and explained for P3HT [9]. Additionally, from the

Stokes prescription, S_2 is a result of specified phase difference between emitting sources, meaning the added sum of all emitting chains (all random within a dropped film) will interfere accordingly and produce off axis polarization (meaning chains that aren't exactly at 45 degrees can contribute additively to the parameter). All of this together allows off axis species (particularly those orientated at ±45º) to emit. Once again, assuming emission along the aggregate axis, the emission can then be interpreted through the Stokes formalism through the S_2 parameter.

The heightened resolution of the S_2 curve can be attributed to a lower exciton population. Because off axis aggregates rely on energy transfer and projection, their excited states are less populated (less excitons are produced), meaning thermal agitation of the transition will have a significantly reduced effect of the subsequent emission, resulting in less broadening of the emission signature. Another possible explanation is a Malu's law (or cosine-squared rule) like interpretation for the emitted FL instead of the incident light, which would suggest a cosine squared dependence as the angle between the excitation and the subsequent emission takes place [3]. This would mean the S_2 parameter should account for 25% or less of the emission, which is easily realized in the inset of Figure 15A (and persists among all acquisitions).

d. Paper 2: Conclusion

H-, J- and HJ-aggregate phenomena are vastly important for the application of semiconducting polymers. Therefore, methods to probe and understand these formations are exceedingly important. The Stokes method outlined above provides a non-invasive and easy to implement measurement technique which can be performed at elevated temperature, allowing those interested to test films and devices cheaply and quickly. We have shown that the Stokes method, when applied to P3HT, can obtain information indicating H-aggregate like formations, which previously could only be obtained via expensive low-temperature measurements. Additionally, we are providing direct evidence to support HJ-aggregate models suggested in literature. We have also shown that local orientation plays a role in the expression / activation of aggregate formations within prepared P3HT films. The heightened resolution provided by the S_2 Stokes parameter could be understood as a combined effect of energy transfer, Malus'

law like excitation and the phase difference introduced to S_2 within the Stokes formalism, continued theoretical calculations and studies are needed to provide verification. Through this S_2 parameter, we have shown that prepared dropped films predominantly display HJ-aggregate formation. However, that excitation conditions and local orientation of polymer chains can affect the expression of H- or HJ-aggregates, suggesting that aggregate types exist, and can be accessed / expressed separately. Following the work of Spano et. Al, we can obtain ratios associated with different aggregates at room temperature, allowing for the acquisition of important film information including correlation length and coherence number. The Stokes technique shows promise in many areas in polymer film production, allowing for a non-invasive and relatively cheap, high temperature probe for film organization and aggregate formation.

e. Paper 2: Figures

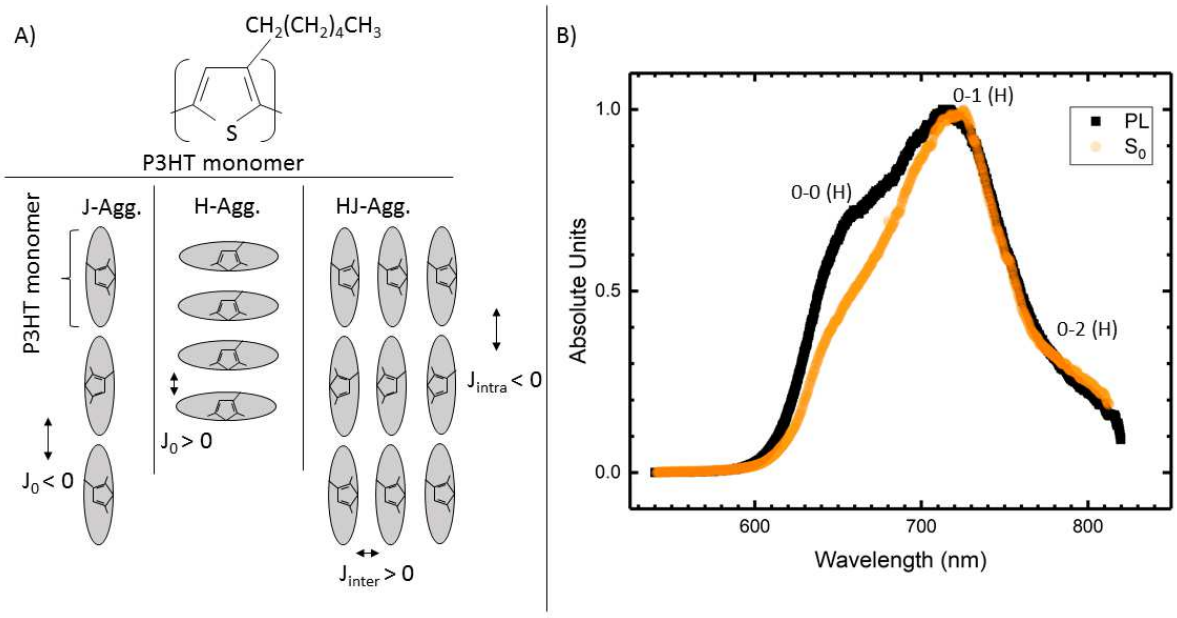

Figure 16. H and J schematic for P3HT and Typical PL Measurement

Figure 16 A) The P3HT repeat monomer is depicted above, with schematic representations of J-, H-, and HJ- aggregate formations shown just below. The coupling constants J0 and Jinter for each formation are shown for clarity. In J-aggregates the 0-0 emission is allowed at low temperature. However, for H and HJ- aggregates, because the coupling constant is greater than zero, excitons populate the $k = \pi$

state, meaning the 0-0 transition must be thermally activated. Subsequent emission can be assumed to be along the axis of the aggregate backbone (the same direction as the arrow indicating the coupling direction).

B) Emission spectra (FL) and Stokes intensity (S0) of P3HT drop cast as described. The spectra agree with typical measurements of P3HT prepared in Chloroform cast as a film. The shouldering in the PL and S0 around 640nm is attributed to the 0-0 H-Aggregate transition. From literature, assignments fall closely to regions around 680nm, 750nm, and 845nm (for the 0-0, 0-1, and 0-2 peak positions respectively) [25, 27, 28, 30, 32]. It is important to note, these assignments are primarily based upon measurements at low temperature, it is expected that the positions will blue shift with temperature, which can be recognized in the assignments to above data.

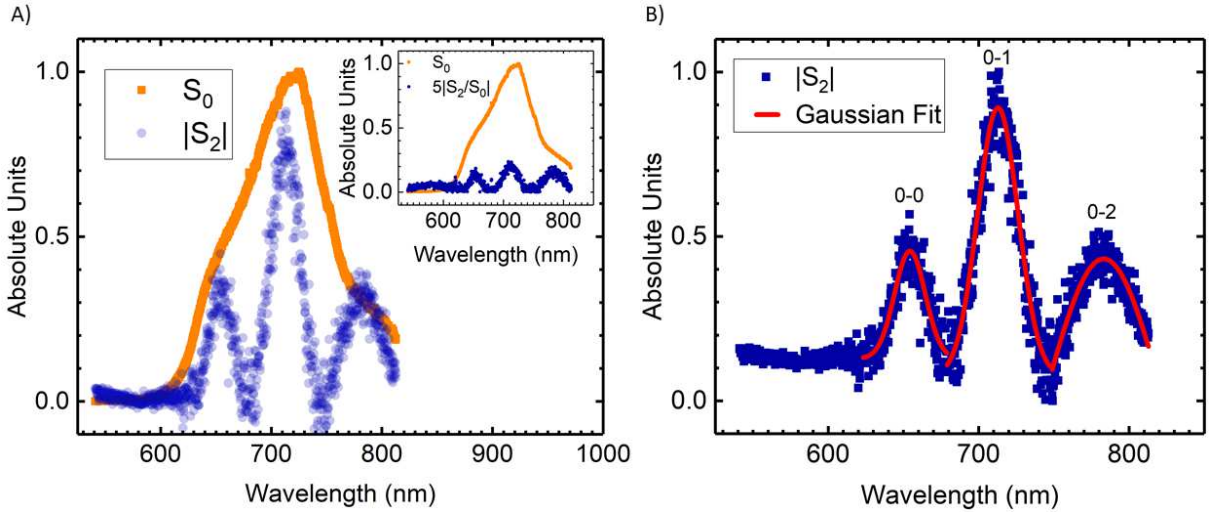

Figure 17. Drop Cast P3HT H-Like behavior

Figure 17 A) Overlay of the overall Stokes intensity (the S0 Stokes parameter) and the S2 parameter (±45º polarization) for the same sample of P3HT described in Figure 16. Here, the individual transition peaks (labeled 0-0, 0-1, and 0-2) can be clearly recognized as those of H-Aggregates in P3HT films and agree well with literature [25, 27, 28, 30, 32]. It is important to note, that S2 has been normalized to its maximum value (normalized to the 0-1 transition) and the modulus taken for clarity,

however S2 for a given transition accounts for less than 30% of the overall emission within its region, the inset is provided to more readily illustrate this point.

B) Example fitting of the S_2 peaks presented in (A). Peak position assignments are based upon literature and displayed. The transition centers correspond well with literature considering blue shift in peak position for H-aggregate spectral signatures with increasing temperature [25, 27, 28, 30, 32]. See Table 2 for more detailed peak information.

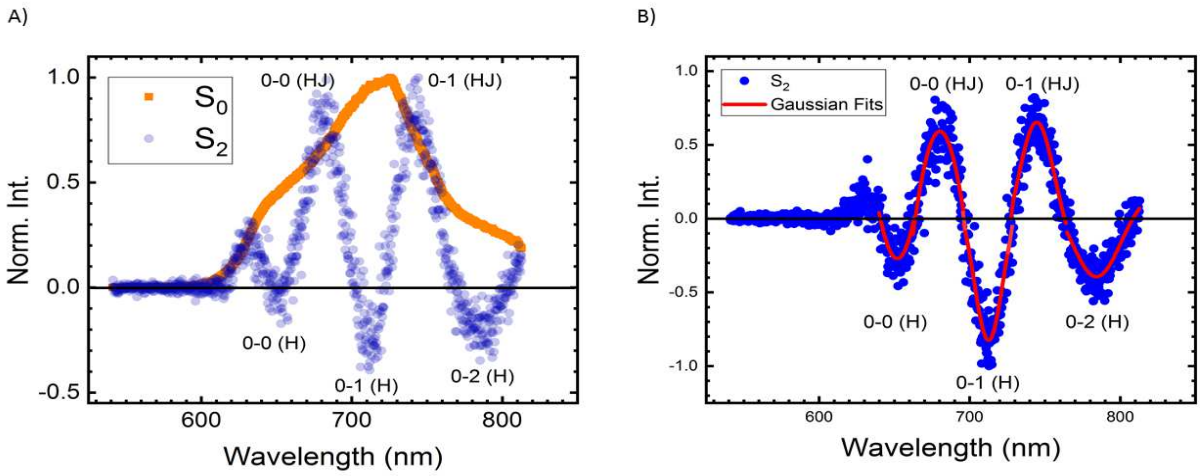

Figure 18. Drop Cast P3HT H- and HJ- Like Behavior

Figure 18 A) Overlay of the Stokes intensity (the S0 Stokes parameter) and the S2 parameter (±45º polarization) for a measurement of drop cast P3HT. This is the same sample and position measured in Figure 17, though the sample has been rotated by 90 degrees. The peak positions are found in the same manner described previously and found to be ~780nm for the 0-0 transition, and ~740nm for the 0-1 transition (labels are provided in the figure). These positions are typical for J-Aggregates in P3HT films and agree well with positions suggested in literature (recall with increasing temperature, J-aggregate signatures are expected to red shift) [25, 27, 28, 30-32, 52]. It is important to note, that S2 has been normalized to its maximum value (in this case the 0-1 (J) transition). The ratio of the 0-0 to the 0-1 peak is lower than suggested in literature [25, 27, 28, 30-32, 52], which suggests that these J-like peaks are

actually affected by J_{inter}, which instead suggests that they are expressions of HJ-aggregate behavior, see Table 1 for more detailed peak information.

B) The S2 parameter (±45º polarization) for a measurement of drop cast P3HT. This is the same sample and position measured in Figure 17 and 18A, although the sample has been rotated by 50 degrees. Here individual transition peaks are labeled 0-0 (H), 0-1 (H) and 0-2 (H) for H-aggregate signatures, and 0-0 (HJ), 0-1 (HJ) for HJ-aggregate signatures. These positions are typical for H and J-Aggregates from P3HT films and agree well with positions suggested in literature (recall with increasing temperature, J-aggregate signatures are expected to red shift while H-aggregates blue shift) [25, 27, 28, 30-32, 52]. Again, because the ratio of what is typically understood as J-aggregate peaks is less than one, we can confirm that J_{inter} is greater than one, and therefore the traditional of J-aggregate peaks is incorrect, therefore these peaks are labeled HJ-. It is important to note, that S2 has been normalized to its maximum negative value (in this case the 0-1 (H) transition). The ratio of the 0-0 to the 0-1 peak for both H- and HJ-aggregates agree with literature, in this case the ratio is found to be ~0.34 for H- aggregates and ~0.91 for J-aggregates [25, 27, 28, 30-32, 52]. See table 1 for more detailed peak information.

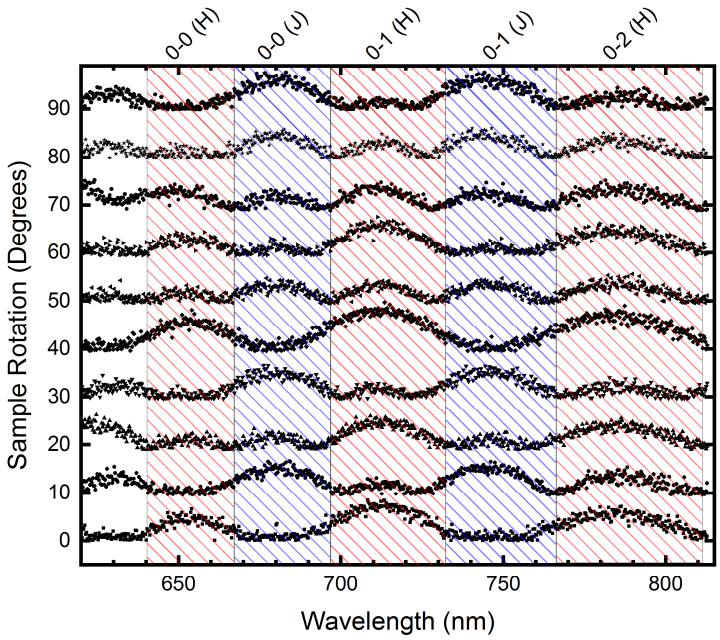

Figure 19. H- J- and HJ- like behavior in P3HT sorted by sample rotation.

Figure 19 The modulus of S2 divided by S0 for the same sample and position measured in Figure 17 and Figure 18 while varying the samples rotation. This graph highlights how, with sample rotation (and therefore local orientation) the expression of exclusively H-, HJ-, and simultaneous expression of H- and HJ- aggregates can be favored following laser excitation in P3HT samples. The approximate range of H and HJ aggregates has been shaded (red for H and blue for HJ) and the transition labeled above the range. Recall, H- (HJ-) aggregate peak positions blue (red) shift with increasing temperature [21, 25-30, 94, 96].

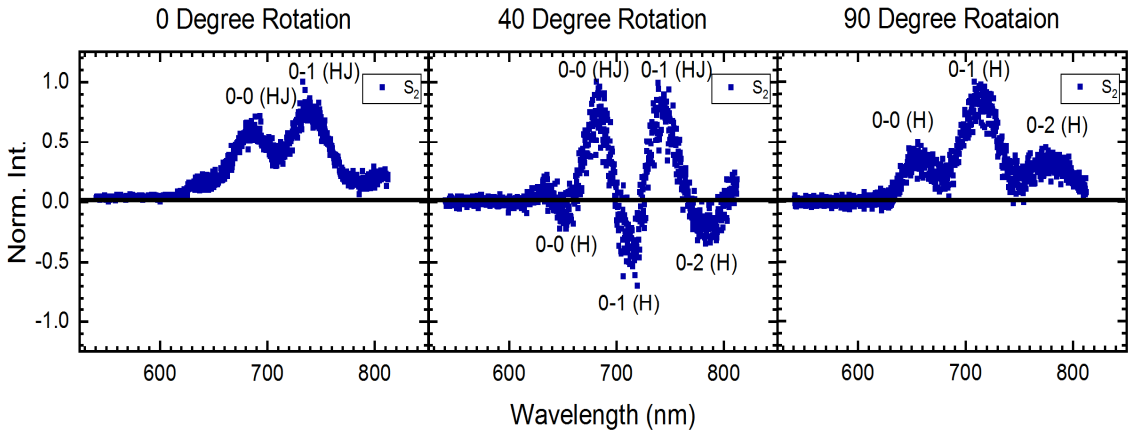

Figure 20. Spin Coated P3HT showing H- J- and HJ- behavior.

Figure 20. Representative S2 acquisitions for spin coated P3HT, measured at the same position but varying sample rotation. Here, from left to right, we can see a spectral transition from purely HJ-type aggregates (at 0 degrees) to an intermediary expression of both H- and HJ- aggregate signatures (at 40 degrees) to purely H-type aggregates (at 90 degrees). Peak positions for H- and HJ- signatures were checked following the gaussian fitting described, and agree with literature, more detailed information can be found in table 2. The ratios of the 0-0 to 0-1 peaks for the zero-degree sample rotation is ~0.7, associated with HJ-aggregates. The 40-degree case find the ratio of the HJ-aggregate peaks to be ~0.94, while the H-aggregate peaks obtain a ratio of 0.24. Finally, the 90-degree sample rotation obtains the H-aggregate ratio to be ~0.4. These peaks are in good agreement with values shown in literature [2, 5, 25, 27, 28, 30-32, 52].

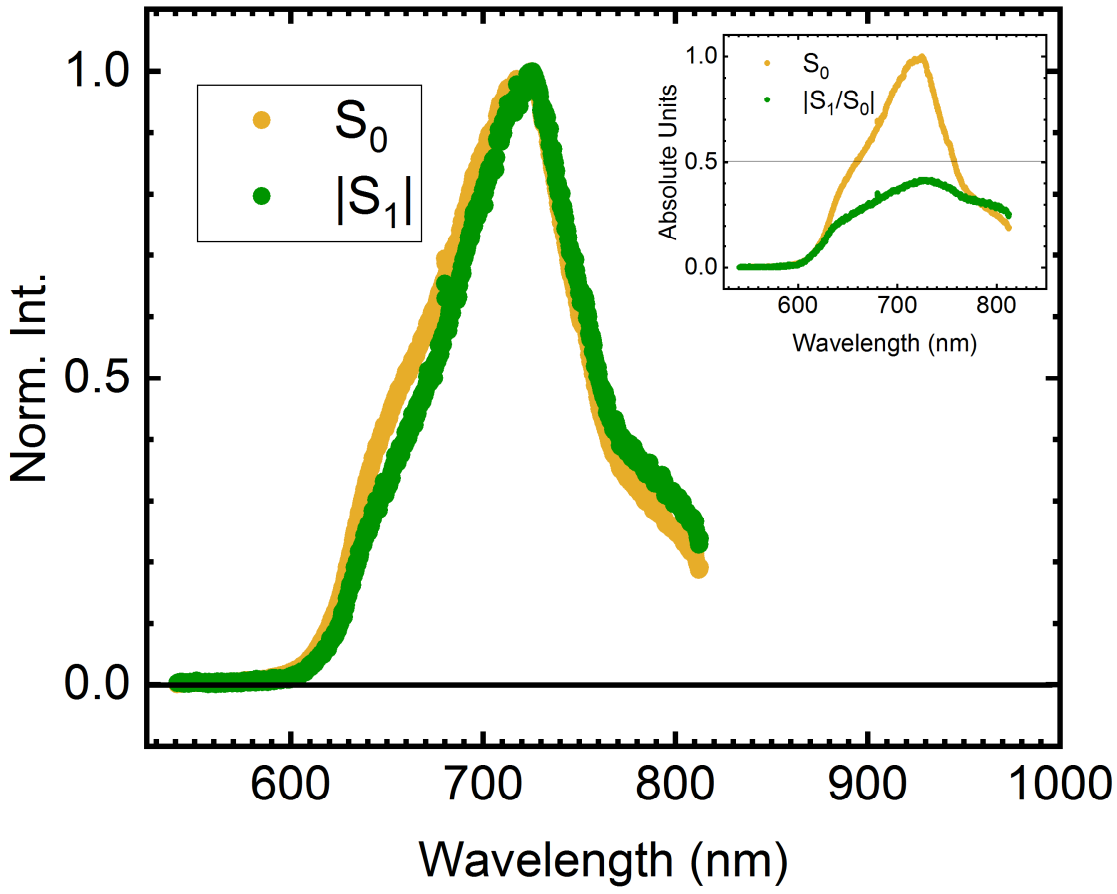

Figure 21. S_0 S_1 Overlay for Drop Cast P3HT

Figure 21. The total intensity Stokes parameter S_0 plotted with the vertically polarized emission S_1. The modulus of S_1 is shown for clarity, however in this case S_1 is negative. S_1 nearly perfectly fits with S_0, expected as the primary excitation (and subsequent emission) of the polymer and aggregate formation should be along the direction of the exciting sources polarization (in this case vertically or $-S_1$) [6]. The inset, shows the modulus of S_1/S_0 and S_0. The ratio helps us understand that approximately 50% of the emission is polarized in this way, the grey line at 0.5 is added to help drive this point (expected for a drop cast sample, as the film can be considered amorphous at long range).

FUTURE WORK

The work of Steyrleuthner et. al. gave us fantastic background on the formations within P(NDI2OD-T2), and suggested that three distinct species can be discerned and tuned through the use of various solvents [37]. These formations, as described in Paper 1, are understood as Isolated chains Aggregate I and Aggregate II species (IC, Agg I and Agg II). The use of "good" solvents promoted IC formation, followed by the distinct formation of Agg I when "worse" solvents such as DiCholorobenzene were and finally Agg II is formed with the worst solvents such as Toluene. However, the most interesting suggestion by this work is that these different formations yield the same type of aggregate, namely H-aggregates.

Separately, the work of Spano *et. al.* provides general method by which absorption and emission spectra can be utilized to describe and measure H- and J- aggregate formation within polymer systems. This set of work relies on the nature of aromatic chains in organic polymers, utilizing much of the H- and J- aggregate quantum mechanical modeling described in chapter 3, to establish fit parameters to describe and relate the peak ratios of H-, J- and HJ- aggregate behavior [24-31]. Of particular use from this series is the assignment of H- and J- aggregates from their emission signatures, with H-aggregates appearing as a series of three distinct peaks at low temperature, whereas J- aggregates display two peaks at low temperature. A more detailed account of this information is provided in Paper 2 above.

A pairing of these two research groups, that is Steyrleuthner *et. al*. and Spano *et. al.,* has yet to be provided. Doing so, according to conventional used, wisdom would traditionally require low-temperature measurements, as aggregate peaks couldn't be elucidated at high temperature. In paper 2, we have shown that the S_2parameter, acquired through the Stokes technique, can provide the heightened resolution needed, even at elevated temperature, to discern such aggregate peaks. This technique has been applied to

P(NDI2OD-T2) across solutions prepared with various solvents, a figure comparing the S_0 and S_2 parameter across solvents can be found in Figure 22. P(NDI2OD-T2) S_0 and S_2 in solution.

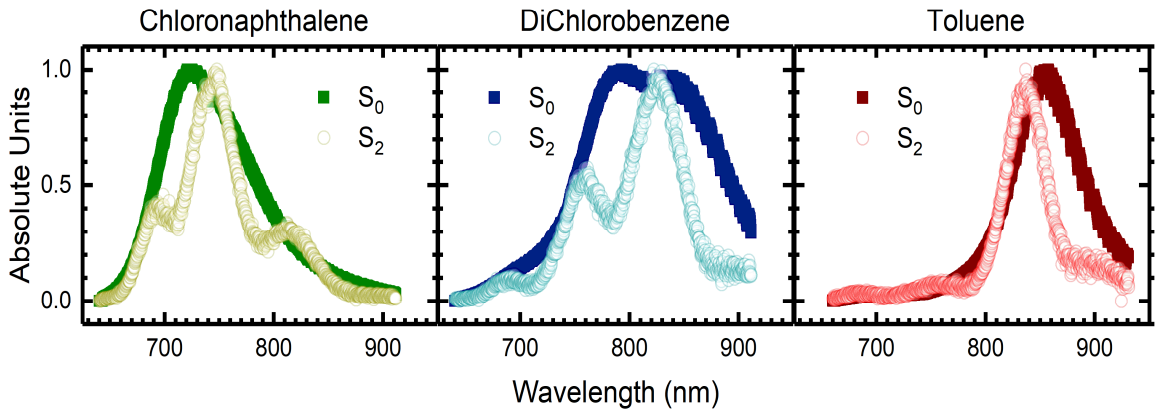

Figure 22. P(NDI2OD-T2) S_0 and S_2 in solution

Here, we present the normalized S_0 and S_2 parameters for prepared solutions of P(NDI2OD-T2) with different solvents (from "Good" to "Bad" solvents). There is nothing surprising about the normalized intensity (S_0) emission, these line shapes agree well with literature [9, 34, 35, 37, 38]. Instead, viewing the S_2 parameter, we can further / clarify assertions made by Steyrleuthner *et. al.* Specifically, we are able to better elucidate aggregate structures where previously, spectral regions were referred to as Isolated Chains (IC), Aggregate species I and II (Agg I and Agg II). It is again of particular importance to note that in this work, it is suggested that all three formations, IC, Agg I and Agg II are of H-aggregate formations. Through application of Stokes Spectroscopy, we find agreement in this assertion, as P(NDI2OD-T2) prepared in solution with a good solvent preferentially forms H-aggregates (again this is generally accepted as the preferential aggregate form) [9, 34, 35, 37, 38]. However, when prepared with a poor solvent, such as DiChlorobenzene (which prompts Agg I formation according to Steyrleuthner et. al.), the solution appears to lose this H-aggregate signature, and takes on a more J-like emission spectrum. This transition to J-aggregates is then fully realized when the worst solvent, Toluene, is utilized. This suggests that the type of aggregate scheme achieved (either H- or J-) can be tuned according to solvent choice

when P(NDI2OD-T2) is prepared in solution, which is in contradiction to previous claims. Spin coating these samples seems to push even the best solvent toward more of a J-like emission spectra when considering the S_2 spectra (see Figure 23 below).

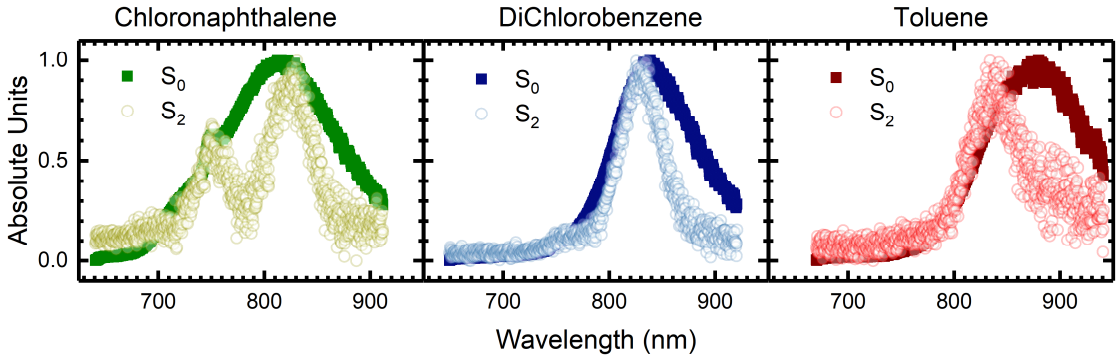

Figure 23. P(NDI2OD-T2) Spin Coated. S_0 S_2 comparison.

This J-like preference found in the S_2 emission spectra for P(NDI2OD-T2), even in a good solvent such as Chloronaphthalene is quite unexpected as groups have previously reported face on stacking of change (H-Like behavior) [35, 37] however may be a result of chains aligning along the radial axis of spun slides due to centrifugal 'force.' Through this initial work, we show that the pairing of aggregate spectral signature suggested by Spano *et. al.* and the aggregate assignment by Steyrleuthner *et. al.* needs to be paired and analyzed simultaneously.

CONCLUDING REMARKS

In this work, I have outlined my contribution to the setup, calibration and initial findings of the Araujo's group spectroscopy lab. This laboratory brings the opportunity for a wide variety of experimental directions and collaborations, spanning soft to condensed matter materials, material characterization to structural elucidation.

The application of Stokes Spectroscopy to the polymer systems P(NDI2OD-T2) and P3HT has been shown through a series of individual papers set for publication and continued preparation. In the first, we showed that broad band polarization spectra can be utilized to determine aggregate formation within P(NDI2OD-T2). Additionally, it was discussed how synthesis considerations including solvent choice and film processing play a role in aggregate formation. Using these considerations, it would be possible to tune the polarization landscape for application purposes.

In the second manuscript, we showed the true strength of Stokes Spectroscopy, bringing a new method of probing aggregate formation within the polymer system P3HT even at elevated temperatures. This finding, when paired with the desire to create new and easily processable organic semiconducting devices, allows researchers to easily identify processing success and failures without having to damage the material itself through traditional measurement techniques. Here we find the true strength of Stokes Spectroscopy: it serves as a non-invasive, optically activated test for material properties, which can easily be added to any existing spectroscopy lab.

Finally, the third manuscript in preparation, shows how Stokes Spectroscopy can be used to further elucidate structural formations within polymer systems. Through its application, we were able to discern different types of aggregate forms previously missed in past studies. Through this discovery, we can suggest that both H- and J- aggregate formations are possible in P(NDI2OD-T2) polymer system, and

the selection of aggregate formation can be prompted through solvent choice.

Stokes Spectroscopy itself has nearly limitless potential, and through continued application and study could serve as a widely utilized measurement technique. Here, we've only touched upon its use in two novel conjugated polymer systems. Prime candidates for additional work includes carbon nanotubes, 2-D materials and other polymer systems (such as P3HT:PCBM blends). Currently, the laboratory group is applying the technique to study 2D chalcogenides, carbon nanotubes, and porphyrin molecules. Additionally, myself in collaboration with Araujo's group will continue to test the application of Stokes Spectroscopy, and have already begun research from the single molecular level to organized solid state materials.

REFERENCES

1. Goldstein, D., *Polarized Light Second Edition, Revised and Expanded.* OPTICAL ENGINEERING-NEW YORK-MARCEL DEKKER INCORPORATED-, 2003. **83**.

2. Goldstein, D.H., *Polarized light*. 2017: CRC press.

3. Halliday, D., R. Resnick, and J. Walker, *Fundamentals of Physics, Chapters 33-37*. 2010: John Wiley & Sons.

4. Pedrotti, F.L. and L.S. Pedrotti, *Introduction to optics 2nd edition.* Introduction to Optics 2nd Edition by Frank L. Pedrotti, SJ, Leno S. Pedrotti New Jersey: Prentice Hall, 1993, 1993.

5. Kuzmany, H., *Solid-state spectroscopy: an introduction*. 2009: Springer Science & Business Media.

6. Valeur, B. and M.N. Berberan-Santos, *Molecular fluorescence: principles and applications*. 2012: John Wiley & Sons.

7. Cimrová, V., et al., *Polarized light emission from LEDs prepared by the Langmuir□Blodgett technique.* Advanced Materials, 1996. **8**(2): p. 146-149.

8. Liang, Y., et al., *50th anniversary perspective: polymeric biomaterials: diverse functions enabled by advances in macromolecular chemistry.* Macromolecules, 2017. **50**(2): p. 483-502.

9. Ostroverkhova, O., *Organic optoelectronic materials: Mechanisms and applications.* Chem. Rev, 2016. **116**(22): p. 13279-13412.

10. Scharf, T., *Polarized light in liquid crystals and polymers*. 2007: John Wiley & Sons.

11. Teale, F., *Principles of Fluorescence Spectroscopy-Lakowicz, Jr*. 1984, MACMILLAN MAGAZINES LTD PORTERS SOUTH, 4 CRINAN ST, LONDON, ENGLAND N1 9XW.

12. Chen, S., et al., *Circularly polarized light generated by photoexcitation of luminophores in glassy liquid-crystal films.* Nature, 1999. **397**(6719): p. 506-508.

13. Hestand, N.J. and F.C. Spano, *Molecular Aggregate Photophysics beyond the Kasha Model: Novel Design Principles for Organic Materials.* Accounts of Chemical Research, 2017. **50**(2): p. 341-350.

14. Kline, R.J., et al., *Controlling the field□effect mobility of regioregular polythiophene by changing the molecular weight.* Advanced Materials, 2003. **15**(18): p. 1519-1522.

15. Laughlin, F.L., *Synthesis and characterization of conjugated materials with phosphorus*. 2013, Case Western Reserve University.

16. Ludwigs, S., *P3ht Revisited-from Molecular Scale to Solar Cell Devices*. 2015: Springer.

17. Salleo, A., *Charge transport in polymeric transistors.* Materials Today, 2007. **10**(3): p. 38-45.

18. Stepto, R., et al., *Mission and challenges of polymer science and technology.* Pure and applied chemistry, 2003. **75**(10): p. 1359-1369.

19. Würthner, F., T.E. Kaiser, and C.R. Saha□Möller, *J□Aggregates: From Serendipitous Discovery to Supramolecular Engineering of Functional Dye Materials.* Angewandte Chemie International Edition, 2011. **50**(15): p. 3376-3410.

20. Yan, H., et al., *A high-mobility electron-transporting polymer for printed transistors.* Nature, 2009. **457**(7230): p. 679-686.

21. Baghgar, M., et al., *Probing inter-and intrachain exciton coupling in isolated poly (3-hexylthiophene) nanofibers: Effect of solvation and regioregularity.* The journal of physical chemistry letters, 2012. **3**(12): p. 1674-1679.

22. Ehrenreich, P., et al., *H-aggregate analysis of P3HT thin films-Capability and limitation of photoluminescence and UV/Vis spectroscopy.* Scientific reports, 2016. **6**: p. 32434.

23. Langeveld-Voss, B., et al., *Circular dichroism and circular polarization of photoluminescence of highly ordered poly {3, 4-di [(S)-2-methylbutoxy] thiophene}*. Journal of the American Chemical Society, 1996. **118**(20): p. 4908-4909.

24. Spano, F.C., *Absorption and emission in oligo-phenylene vinylene nanoaggregates: The role of disorder and structural defects.* The Journal of chemical physics, 2002. **116**(13): p. 5877-5891.

25. Spano, F.C., *Modeling disorder in polymer aggregates: The optical spectroscopy of regioregular poly (3-hexylthiophene) thin films.* The Journal of chemical physics, 2005. **122**(23): p. 234701.

26. Spano, F.C., *Excitons in conjugated oligomer aggregates, films, and crystals.* Annu. Rev. Phys. Chem., 2006. **57**: p. 217-243.

27. Spano, F.C., *The spectral signatures of Frenkel polarons in H-and J-aggregates.* Accounts of chemical research, 2009. **43**(3): p. 429-439.

28. Spano, F.C., et al., *Determining exciton coherence from the photoluminescence spectral line shape in poly (3-hexylthiophene) thin films.* The Journal of chemical physics, 2009. **130**(7): p. 074904.

29. Spano, F.C., et al., *Probing excitation delocalization in supramolecular chiral stacks by means of circularly polarized light: experiment and modeling.* Journal of the American Chemical Society, 2007. **129**(22): p. 7044-7054.

30. Spano, F.C. and C. Silva, *H-and J-aggregate behavior in polymeric semiconductors.* Annual review of physical chemistry, 2014. **65**: p. 477-500.

31. Spano, F.C. and H. Yamagata, *Vibronic coupling in J-aggregates and beyond: a direct means of determining the exciton coherence length from the photoluminescence spectrum.* The Journal of Physical Chemistry B, 2010. **115**(18): p. 5133-5143.

32. Yamagata, H. and F.C. Spano, *Interplay between intrachain and interchain interactions in semiconducting polymer assemblies: The HJ-aggregate model.* The Journal of chemical physics, 2012. **136**(18): p. 184901.

33. Zen, A., et al., *Effect of molecular weight and annealing of poly (3□hexylthiophene) s on the performance of organic field□effect transistors.* Advanced Functional Materials, 2004. **14**(8): p. 757-764.

34. Anton, A.M., et al., *Spatial Orientation and Order of Structure-Defining Subunits in Thin Films of a High Mobility n-Type Copolymer.* Macromolecules, 2016. **49**(5): p. 1798-1806.

35. Rivnay, J., et al., *Unconventional Face□On Texture and Exceptional In□Plane Order of a High Mobility n□Type Polymer.* Advanced Materials, 2010. **22**(39): p. 4359-4363.

36. Sciascia, C., et al., *Sub□Micrometer Charge Modulation Microscopy of a High Mobility Polymeric n□Channel Field□Effect Transistor.* Advanced Materials, 2011. **23**(43): p. 5086-5090.

37. Steyrleuthner, R., et al., *Aggregation in a high-mobility n-type low-bandgap copolymer with implications on semicrystalline morphology.* Journal of the American Chemical Society, 2012. **134**(44): p. 18303-18317.

38. Zerson, M., et al., *Surface Structure of Semicrystalline Naphthalene Diimide–Bithiophene Copolymer Films Studied with Atomic Force Microscopy.* Macromolecules, 2016. **49**(17): p. 6549-6557.

39. Atkins, P. and J. de Paula, *Chemical equilibrium.* Atkins' physical chemistry, 7th edn. Oxford University Press, Oxford, UK, 2002: p. 222-251.

40. Jablonski, A., *Efficiency of anti-Stokes fluorescence in dyes.* Nature, 1933. **131**(839-840): p. 21.

41. Labastide, J.A., et al., *Time-and polarization-resolved photoluminescence decay from isolated polythiophene (P3HT) nanofibers.* The Journal of Physical Chemistry C, 2012. **116**(44): p. 23803-23811.

42. Mikhnenko, O.V., P.W. Blom, and T.-Q. Nguyen, *Exciton diffusion in organic semiconductors.* Energy & Environmental Science, 2015. **8**(7): p. 1867-1888.

43. Brown, S.J., et al., *Morphology-dependent optical anisotropies in the n-type polymer P (NDI2OD-T2).* Physical Review B, 2016. **94**(16): p. 165105.

44. Giussani, E., et al., *Molecular level investigation of the film structure of a high electron mobility copolymer via vibrational spectroscopy.* Macromolecules, 2013. **46**(7): p. 2658-2670.

45. Schuettfort, T., et al., *Surface and bulk structural characterization of a high-mobility electron-transporting polymer.* Macromolecules, 2011. **44**(6): p. 1530-1539.

46. Arthur Markus Anton, R.S., Wilhelm Kossack, Dieter Neher, and Friedrich Kremer, *Spatial Orientation and Order of Structure-Defining Subunits in Thin Films of a High Mobility n-Type Copolymer.* Macromolecules, 2016. **49**(5): p. 1798-1806.

47. Chen, Z., Stepanenko, V., Dehm, V., Prins, P., Siebbeles, Laurens D. A., Seibt, J., Marquetand, P., Engel, V. and Würthner, F. , *Photoluminescence and Conductivity of Self-Assembled π–π Stacks of Perylene Bisimide Dyes.* Chem. Eur. J., 2007. **13**: p. 436–449.

48. Donley, C.L., et al., *Effects of Packing Structure on the Optoelectronic and Charge Transport Properties in Poly (9, 9-di-n-octylfluorene-alt-benzothiadiazole).* Journal of the American Chemical Society, 2005. **127**(37): p. 12890-12899.

49. Jimison, L.H., et al., *Charge□Transport Anisotropy Due to Grain Boundaries in Directionally Crystallized Thin Films of Regioregular Poly (3□hexylthiophene).* Advanced Materials, 2009. **21**(16): p. 1568-1572.

50. Kline, R.J., et al., *Dependence of regioregular poly (3-hexylthiophene) film morphology and field-effect mobility on molecular weight.* Macromolecules, 2005. **38**(8): p. 3312-3319.

51. Robert Steyrleuthner, M.S., Ian Howard, Bastian Klaumünzer, Kristian Schilling, Zhihua Chen, Peter Saalfrank, Frédéric Laquai, Antonio Facchetti, and Dieter Neher, *Aggregation in a High-Mobility n-Type Low-Bandgap Copolymer with Implications on Semicrystalline Morphology.* Journal of the American Chemical Society 2012. **134**(44): p. 18303-18317.

52. Baghgar, M., et al., *Effect of polymer chain folding on the transition from H-to J-aggregate behavior in P3HT nanofibers.* The Journal of Physical Chemistry C, 2014. **118**(4): p. 2229-2235.

53. Panzer, F., et al., *Spectroscopic signature of two distinct H-aggregate species in poly (3-hexylthiophene).* Macromolecules, 2015. **48**(5): p. 1543-1553.

54. Lin, J.W.P. and L.P. Dudek, *Synthesis and properties of poly (2, 5□thienylene).* Journal of Polymer Science Part A: Polymer Chemistry, 1980. **18**(9): p. 2869-2873.

55. McCullough, R.D. and R.D. Lowe, *Enhanced electrical conductivity in regioselectively synthesized poly (3-alkylthiophenes).* Journal of the Chemical Society, Chemical Communications, 1992(1): p. 70-72.

56. McCullough, R.D., et al., *Design, synthesis, and control of conducting polymer architectures: structurally homogeneous poly (3-alkylthiophenes).* The Journal of Organic Chemistry, 1993. **58**(4): p. 904-912.

57. Pommerehne, J., et al., *Efficient two layer leds on a polymer blend basis.* Advanced Materials, 1995. **7**(6): p. 551-554.

58. Cardona, C.M., et al., *Electrochemical considerations for determining absolute frontier orbital energy levels of conjugated polymers for solar cell applications.* Advanced materials, 2011. **23**(20): p. 2367-2371.

59. Heffner, G.W. and D.S. Pearson, *Molecular characterization of poly (3-hexylthiophene).* Macromolecules, 1991. **24**(23): p. 6295-6299.

60. Chen, T.-A., X. Wu, and R.D. Rieke, *Regiocontrolled synthesis of poly (3-alkylthiophenes) mediated by Rieke zinc: their characterization and solid-state properties.* Journal of the American Chemical Society, 1995. **117**(1): p. 233-244.

61. Mao, H., B. Xu, and S. Holdcroft, *Synthesis and structure-property relationships of regioirregular poly (3-hexylthiophenes).* Macromolecules, 1993. **26**(5): p. 1163-1169.

62. Xu, B. and S. Holdcroft, *Molecular control of luminescence from poly (3-hexylthiophenes).* Macromolecules, 1993. **26**(17): p. 4457-4460.

63. Ihn, K.J., J. Moulton, and P. Smith, *Whiskers of poly (3□alkylthiophene) s.* Journal of Polymer Science Part B: Polymer Physics, 1993. **31**(6): p. 735-742.

64. Samitsu, S., et al., *Effective production of poly (3-alkylthiophene) nanofibers by means of whisker method using anisole solvent: structural, optical, and electrical properties.* Macromolecules, 2008. **41**(21): p. 8000-8010.

65. Liu, J., et al., *Controlling poly (3-hexylthiophene) crystal dimension: nanowhiskers and nanoribbons.* Macromolecules, 2009. **42**(24): p. 9390-9393.

66. Niles, E.T., et al., *J-aggregate behavior in poly-3-hexylthiophene nanofibers.* The Journal of Physical Chemistry Letters, 2012. **3**(2): p. 259-263.

67. Bardeen, C.J., *The structure and dynamics of molecular excitons.* Annual review of physical chemistry, 2014. **65**: p. 127-148.

68. Kogo, K., et al., *Polarized light emission from a calamitic liquid crystalline semiconductor doped with dyes.* Applied physics letters, 1998. **73**(11): p. 1595-1597.

69. Ren, M., et al., *Linearly polarized light emission from quantum dots with plasmonic nanoantenna arrays.* Nano letters, 2015. **15**(5): p. 2951-2957.

70. Konishi, K., et al., *Circularly polarized light emission from semiconductor planar chiral nanostructures.* Physical review letters, 2011. **106**(5): p. 057402.

71. Li, P., et al., *Polarized incandescent light emission from carbon nanotubes.* Applied physics letters, 2003. **82**(11): p. 1763-1765.

72. Alliprandini-Filho, P., et al., *Induced Secondary Structure in Nanostructured Films of Poly (p-phenylene vinylene).* Journal of nanoscience and nanotechnology, 2009. **9**(10): p. 5981-5989.

73. Chen, Z., et al., *Photoluminescence and Conductivity of Self□Assembled π–π Stacks of Perylene Bisimide Dyes.* Chemistry-A European Journal, 2007. **13**(2): p. 436-449.

74. Alliprandini Filho, P., et al., *Emission ellipsometry used to probe aggregation of the luminescent 2, 1, 3-benzothiadiazole dyes and ordering in an E7 liquid crystal matrix.* Physical Chemistry Chemical Physics, 2014. **16**(7): p. 2892-2896.

75. Basilio, F.C., et al., *Ellipsometric Raman Spectroscopy.* The Journal of Physical Chemistry C, 2016. **120**(43): p. 25101-25109.

76. Therézio, E.M., et al., *Light polarization states of a cholesteric liquid crystal probed with optical ellipsometry.* Optical Materials, 2015. **48**: p. 7-11.

77. Kittel, C. and H. Kroemer, *Thermal Physics, 473 pp*. 1980, WH Freeman, New York.

78. Capaz, R. and M. Caldas, *Ab initio calculations of structural and dynamical properties of poly (p-phenylene) and poly (p-phenylene vinylene).* Physical Review B, 2003. **67**(20): p. 205205.

79. Marletta, A., et al., *Rapid Conversion of Poly (p□phenylenevinylene) Films at Low Temperatures.* Advanced Materials, 2000. **12**(1): p. 69-74.

80. Silva, H.S., et al., *Controlling Bandgap Energy and Multivibronic Modes of a Poly (2, 5-thiophene-1, 4-dialkoxyphenylene) Derivative by Gamma Photons.* The Journal of Physical Chemistry A, 2011. **115**(29): p. 8288-8294.

81. Borissevitch, I.E., *More about the inner filter effect: corrections of Stern–Volmer fluorescence quenching constants are necessary at very low optical absorption of the quencher.* Journal of luminescence, 1999. **81**(3): p. 219-224.

82. Takacs, C.J., et al., *Mapping orientational order in a bulk heterojunction solar cell with polarization-dependent photoconductive atomic force microscopy.* ACS nano, 2014. **8**(8): p. 8141-8151.

83. Takacs, C.J., et al., *Remarkable order of a high-performance polymer.* Nano letters, 2013. **13**(6): p. 2522-2527.

84. Goldstein, D., *Polarized Light second exition, revised and expanded*. 2003, New York, New York: Marcel Dekker.

85. Handa, N.V., et al., *Exploring the synthesis and impact of end□functional poly (3□hexylthiophene).* Journal of Polymer Science Part A: Polymer Chemistry, 2015. **53**(7): p. 831-841.

86. Hestand, N.J., et al., *Exciton mobility control through sub− Å packing modifications in molecular crystals.* Physical Review B, 2015. **91**(19): p. 195315.

87. Kilina, S., D. Kilin, and S. Tretiak, *Light-driven and phonon-assisted dynamics in organic and semiconductor nanostructures.* Chemical reviews, 2015. **115**(12): p. 5929-5978.

88. Musto, P., *Grand challenges in polymer chemistry: energy, environment, health.* Frontiers in chemistry, 2013. **1**.

89. Wang, D., et al., *From single chains to aggregates, how conjugated polymers behave in dilute solutions.* Macromolecules, 2013. **46**(15): p. 6217-6224.

90. Scharsich, C., et al., *Control of aggregate formation in poly (3□hexylthiophene) by solvent, molecular weight, and synthetic method.* Journal of Polymer Science Part B: Polymer Physics, 2012. **50**(6): p. 442-453.

91. Manas, E.S. and F.C. Spano, *Absorption and spontaneous emission in aggregates of conjugated polymers.* The Journal of chemical physics, 1998. **109**(18): p. 8087-8101.

92. Nakano, T., *Synthesis, structure and function of π-stacked polymers.* Polymer journal, 2010. **42**(2): p. 103-123.

93. Traiphol, R., et al., *Chain organization and photophysics of conjugated polymer in poor solvents: aggregates, agglomerates and collapsed coils.* Polymer, 2007. **48**(3): p. 813-826.

94. Yamagata, H., et al., *HJ-aggregate behavior of crystalline 7, 8, 15, 16-tetraazaterrylene: Introducing a new design paradigm for organic materials.* The Journal of Physical Chemistry C, 2014. **118**(49): p. 28842-28854.

95. Noriega, R., et al., *A general relationship between disorder, aggregation and charge transport in conjugated polymers.* Nature materials, 2013. **12**(11): p. 1038-1044.

96. Kistler, K., et al., *Absorption, circular dichroism, and photoluminescence in perylene diimide bichromophores: Polarization-dependent H-and J-aggregate behavior.* The Journal of Physical Chemistry B, 2011. **116**(1): p. 77-86.